Constraining spectral models of a terrestrial gamma-ray flash from a terrestrial electron beam observation by the Atmosphere-Space Interactions Monitor

David Sarria[1,1], Nikolai Østgaard[2,2], Pavlo Kochkin[3,3], Nikolai Lehtinen [3,3], Andrew Mezentsev[4,4], Martino Marisaldi[3,3], Anders Lindanger[1,1], Carolina Maiorana[1,1], Brant Edward Carlson[5,5], Torsten Neubert[6,6], Víctor Reglero[7,7], Kjetil Ullaland[1,1], Shiming Yang[1,1], Georgi Genov[1,1], Bilal Hasan Qureshi[8,8], Carl Budtz-Jørgensen[9,9], Irfan Kuvvetli[6,6], Freddy Cristiansen[10,10], Olivier Chanrion[11,11], Javier Navarro-Gonzalez[7,7], Paul Henry Connell[7,7], and Christopher J Dr Eyles[12,12]

[1]Birkeland Centre for Space Science, University of Bergen
[2]Birkeland Centre for Space Science,University of Bergen
[3]University of Bergen
[4]Birkeland Centre for Space Science
[5]Carthage College
[6]Department of Solar System Physics, Denmark
[7]University of Valencia
[8]Department of Physics and Technology, University of Bergen
[9]Technical University of Denmark
[10]DTU Space
[11]National Space Institute (DTU Space)
[12]University of Birmingham

November 30, 2022

Abstract

Terrestrial Gamma-ray Flashes (TGFs) are short flashes of high energy photons, produced by thunderstorms. When interacting with the atmosphere, they produce relativistic electrons and positrons, and a part gets bounded to geomagnetic field lines and travels large distances in space. This phenomenon is called a Terrestrial Electron Beam (TEB). The Atmosphere-Space Interactions Monitor (ASIM) mounted on-board the International Space Station detected a new TEB event on March 24, 2019, originating from the tropical cyclone Johanina. Using ASIM's low energy detector, the TEB energy spectrum is resolved down to 50 keV. We provide a method to constrain the TGF source spectrum based on the detected TEB spectrum. Applied to this event, it shows that only fully developed RREA spectra are compatible with the observation. More specifically, assuming a TGF spectrum [?] 1/E exp(-E/ε), the compatible models have ε [?] 6.5 MeV (E is the photon energy and ε is the cut-off energy). We could not exclude models with ε of 8 and 10 MeV.

Constraining spectral models of a terrestrial gamma-ray flash from a terrestrial electron beam observation by the Atmosphere-Space Interactions Monitor

D. Sarria[1], N. Østgaard[1], P. Kochkin[1], N. Lehtinen[1], A. Mezentsev[1], M. Marisaldi[1], A. Lindanger[1], C. Maiorana[1], B. E. Carlson[1,2], T. Neubert[3], V. Reglero[4], K. Ullaland[1], S.Yang[1], G. Genov[1], B. H. Qureshi[1], C. Budtz-Jørgensen[3], I. Kuvvetli[3], F. Christiansen[3], O. Chanrion[3], J. Navarro-González[4], P. Connel[4], C. Eyles[4]

[1]Birkeland Centre for Space Science, University of Bergen, Bergen, Norway
[2]Carthage College, Kenosha, Wisconsin, United States
[3]National Space Institute, Technical University of Denmark, Lyngby, Denmark
[4]University of Valencia, Valencia, Spain

Key Points:

- Observation of a Terrestrial Electron Beam with a spectrum resolved down to 50 keV
- A method to constrain the energy spectrum of the source Terrestrial Gamma-ray Flash based on the detection of the associated TEB is presented
- Only TGFs originating from fully-developed RREA models can explain the observation

Corresponding author: D. Sarria, `david.sarria@uib.no`

Abstract

Terrestrial Gamma-ray Flashes (TGFs) are short flashes of high energy photons, produced by thunderstorms. When interacting with the atmosphere, they produce relativistic electrons and positrons, and a part gets bounded to geomagnetic field lines and travels large distances in space. This phenomenon is called a Terrestrial Electron Beam (TEB). The Atmosphere-Space Interactions Monitor (ASIM) mounted on-board the International Space Station detected a new TEB event on March 24, 2019, originating from the tropical cyclone Johanina. Using ASIM's low energy detector, the TEB energy spectrum is resolved down to 50 keV. We provide a method to constrain the TGF source spectrum based on the detected TEB spectrum. Applied to this event, it shows that only fully developed RREA spectra are compatible with the observation. More specifically, assuming a TGF spectrum $\propto E^{-1}\exp(-E/\epsilon)$, the compatible models have $\epsilon \geq 6.5$ MeV (E is the photon energy and ϵ is the cut-off energy). We could not exclude models with ϵ of 8 and 10 MeV.

Plain Language Summary

Terrestrial Gamma-ray Flashes (TGF), originating from thunderstorms, are the highest energy natural particle acceleration phenomena occurring on Earth. The production mechanism of TGFs is not very well understood. When interacting with the atmosphere, TGFs produce secondary electrons and positrons, and a part gets bounded to Earth's magnetic field lines, and travels large distances in space. They can be detected by instruments on-board satellites located at the right place (in a window of about 40 km) at the right time (in a window of a few milliseconds). This phenomenon is called a Terrestrial Electron Beam (TEB). By detecting the TEB, we can retrieve information about the TGF that produced it. In this article we present the first TEB originating from a tropical cyclone, and with the lowest energies ever recorded (down to 50 keV). We also provide a method to infer properties of the energy distribution of the TGF (producing the TEB) based on the energy spectrum of the TEB. Applied to this event, it shows that only TGF energy spectra among the most energetic that were proposed are compatible, and we cannot exclude even more energetic events.

1 Introduction

Terrestrial Gamma-ray Flashes (TGFs) are short bursts of high energy ($<$ 40 MeV) photons, produced during thunderstorms. A review of TGFs theory and observations is presented by Dwyer et al. (2012). TGFs were first detected using the BATSE experiment on-board the CGRO spacecraft (Fishman et al., 1994). Later, TGFs were recorded by the satellites RHESSI (Smith et al., 2005), AGILE (Marisaldi et al., 2014), Fermi (Briggs et al., 2010; Roberts et al., 2018), BeppoSAX (Ursi et al., 2017) and the Atmosphere-Space Interactions Monitor (ASIM) (Neubert, Østgaard, Reglero, Blanc, et al., 2019). ASIM was successfully launched and docked to the International Space Station in April 2018, and started science operations since June 2018. The first results from ASIM were presented by Østgaard, Neubert, et al. (2019); Sarria et al. (2019); Neubert, Østgaard, Reglero, Chanrion, et al. (2019).

When referring to "electrons beams" in the context of TGFs, one can think of two different objects. The first is associated with the production process of the TGF. This production process takes place, at least for TGF detectable from space, between ≈10 and ≈15 km altitude. This first type of "electron beam" consists of the Relativistic Runaway Electron Avalanche (RREA) producing the TGF's high energy photons. This RREA is not detectable from space since it is is impossible for it to go through the atmosphere layer. The second type of "electron beam" is called "terrestrial electron beam" (TEB) and is produced higher in the atmosphere by the TGF's photons, though the processes of Compton scattering and electron-positron pair production. Since electron-positron pair production is involved, TEBs are composed of a fraction of positrons, typically 10 % to 30 % (see Briggs et al. (2011), table 1). A TEB is bound ("beamed") around the magnetic field line intercepting the source TGF's geographical location (Dwyer et al., 2008; Cohen et al., 2010; Sarria et al., 2015). Most electrons and positrons forming TEBs are produced above 40 km altitude, where the air collision frequency of the electrons (and positrons) is comparable to their gyration frequency around geomagnetic field lines. TEBs propagate in space and travel large distances in the magnetosphere. TEBs were first reported from measurements of the CGRO spacecraft (Dwyer et al., 2008). Later, they were detected by Fermi (Briggs et al., 2011; Stanbro et al., 2019), BeppoSAX (Ursi et al., 2017), AGILE (Lindanger et al., 2020) and ASIM (Sarria et al., 2019). RHESSI probably detected one or two TEB event(s), but it has not been 100% confirmed yet (Smith et al., 2006; Gjesteland, 2012). In general, TEBs are detected much less often than TGFs (e.g.

Fermi has a few thousand TGFs and about 30 TEBs) because the detector must be located inside a narrow window of less than a few tens of kilometers along the right geomagnetic field line (intercepting the TGF source position), and they last for only a few milliseconds.

One of the reasons of studing TEBs is to retrieve information about the TGFs that produced them. Briggs et al. (2011) constrained the positron fraction to be between 10 and 34%, based on 3 events. Positrons fractions are linked to the spectral shape of the source TGF, as photons with harder specturms will do more pair production. In Sarria et al. (2019), the beaming of the source TGF could be constrained between about 30^o and 42^o (half angle, isotropic within a cone). Another reason to study TEBs is that they may have an impact on the inner Van Allen radiation belt, that has not been quantified yet (to our knowledge). Even if it is an important question, it is not the subject of the present paper.

One of the most important question regarding TGFs is their production mechanism. Two main models are proposed to explain the production of TGFs, and in both, the TGF's photons are produced by high energy electrons through the bremsstrahlung process. These high energy electrons form a Relativistic Runaway Electron Avalanche (RREA) (Wilson, 1924; Gurevich et al., 1992). In the first model, a large scale electric field within thunderclouds is considered. This requires the presence of initial high energy seed electrons, that may be provided by cosmic-ray secondaries or background radiation. The background electric field is strong enough to produce RREA avalanches, but the RREA mechanism alone is not enough to produce bright enough TGFs (i.e. detectable from space, therefore with more than 10^{16} photons between 50 keV and 40 MeV at source), and a x-ray and positron feedback mechanism is required (the "relativistic feedback"); only possible if large potentials are available (Dwyer et al., 2003; Babich et al., 2005; Dwyer, 2012; Skeltved et al., 2014). This mechanism will produce a discharge of the thundercloud, that is of different nature than usual lightning discharges. The resulting high-energy photon spectrum given by this model is a so-called "fully-developed" RREA. The development of a RREA process can be characterized by the number of avalanche lengths that were achieved (that depends on the extend and magnitude of the available electric potential). The energy spectrum of the electrons converges to a standard shape ($\approx \exp(-E/7.3\text{MeV})$), which is fully obtained with six or more avalanche lengths, even if the total number of electrons keeps exponentially increasing with the number of avalanche lengths. Another variant of this model uses a lightning leader to push the background (large scale) field above the threshold to trigger the relativistic feedback mechanism (Skeltved et al., 2017).

The second model of TGF production requires a propagating lightning leader. It is sometimes referred as the "leader-streamer" model. It considers that initial seed electrons are produced by the cold runaway mechanism (Gurevich, 1961), happening in the streamer phase or in the leader phase (Moss et al., 2006; Dwyer, 2008; Celestin & Pasko, 2011; Chanrion et al., 2014; Kohn & Ebert, 2015). These energetic seed electrons follow a specific distribution and a fraction of them are then accelerated and multiplied by a larger scale electric field, producing a RREA. The larger scale electric field can be the field induced by the leader and/or a large scale (background) field in the thunderstorm. In principle, leader-based TGF production models do not exclude the possibility of relativistic feedback, that could be more or less important (Skeltved et al., 2017). A parameter that impacts the energy spectrum of emitted photons the most is the potential drop in the leader tip region that is available for the acceleration of energetic electrons. Resulting TGF energy spectra for several leader potential drops are presented in Celestin et al. (2015), figure 3. They actually correspond to a more or less developed RREA process. Celestin et al. (2012) also showed that energy spectra harder than this characteristic fully-developed RREA spectrum could be achieved by involving non-equilibrium acceleration of electrons. One significant advantage of leader-based TGF models is that they propose an unified approach to explain TGF's X/gamma-ray production, as well as x-ray (i.e. softer) emissions from lightning propagating leaders, that were observed from ground, balloons and aircraft (Dwyer et al., 2003, 2004, 2005, 2011). Mailyan et al. (2019) presented the first study that confronted leader models to TGFs recorded by the Fermi space telescope, with tested potential drops $\leq$ 200 MV. They found that lightning leader models with potentials of 200 MV and tilted beams gave the best fit to the data in most of the analyzed TGF events. However, the range of compatible models is found to be quite wide.

In this article, we report the second TEB event detected by ASIM on 24 March 2019. Compared to the previous event (presented in Sarria et al. (2019)), data from the two detectors are available: the pixelated Low-Energy detector (50-400 keV) and the High Energy Detector (300 keV-30 MeV), that permits an unprecedented spectral analysis of a TEB event. In section 2, we present the instruments that were used. In section 3 we present the event. In section 4 we present the methods and models we use for the spectral analysis. In section 5 we show the results of the analysis. We conclude in section 6.

2 Instruments

The ASIM payload (Neubert, Østgaard, Reglero, Blanc, et al., 2019) consists of two main instruments, the Modular X- and Gamma-ray Sensor (MXGS) (Østgaard, Balling, et al., 2019) and the Modular Multi-spectral Imaging Array (MMIA) (Chanrion et al., 2019). ASIM is mounted on the International Space Station (ISS) orbiting the Earth at about 400 kilometers altitude with an inclination of 51.6^o. MXGS consists of two detectors for detecting X- and gamma-rays. The MXGS Low-Energy Detector (LED) is layer of 16384 pixels of Cadmium-Zink-Telluride (CZT) detector crystals, sensitive to photons with energies from 50 keV to about 400 keV. The MXGS High Energy Detector (HED) comprises 12 Bismuth-Germanium-Oxide (BGO) detector modules coupled to photomultiplier tubes (PMT), sensitive in the energy range of 300 keV to about 40 MeV.

GLD360 (VAISALA) is a network of ground-based lightning sensors (1 kHz-350 kHz) detecting both Cloud-to-Groung and Intra-Cloud lightning. The GLD360 sensors use a combination of magnetic direction finding and time-of-arrival calculations (from 4 stations or more) to geolocate the lightning source (see acknowledgments for more details). The typical uncertainty on location is about 2.5 km and it can vary a lot with geographical location (Rudlosky et al., 2017).

We also present data provided by the Meteosat-11 geostationary satellite, that provides regular scans of cloud coverage at several wavelengths (used data comes from band 4, at 3.9 μm, with a 3 km spatial resolution). See acknowledgments for more information.

3 Observation

Figure 1 shows a map of the event together with Satellite imagery that was provided by the geostationary satellite Meteosat-11. The ASIM trigger UTC time is 2019-Mar-24 00:31:53.135444 and the ISS was located at latitude of $\phi = 0.157^o$, longitude of $\lambda = 55.301^o$ and altitude of $h = 408.6$ km, that is above the Indian ocean, close to Madagascar. The ASIM clock has a -20 to 30 ms absolute timing uncertainty with respect to GPS UTC time. A VAISALA (GLD360) discharge event with a UTC time of

2019-03-24 00:31:53.134000 ($\Delta t = 1.44$ ms) was found very close to the southern magnetic line footpoint (at 45 km altitude) intercepting the ISS position : [$\phi_{GLD360} = -7.049^o$, $\lambda_{GLD360} = 55.912^o$] and [$\phi_{mag,s} = -7.007^o$, $\lambda_{mag,s} = 55.923^o$] that gives $\Delta r = 4.82$ km. Note that the GLD360 location uncertainty can be up to 20 km for this event, and the uncertainty in the ISS position is of the same order. The northern magnetic field line footpoint is located at [$\phi_{mag,n} = 20.524^o$, $\lambda_{mag,n} = 55.099^o$], but no lightning activity was observed close to it. No lightning activity was detected by GLD360 below the ISS, within 540 km and ± 1 second around the trigger time. The MMIA photometers did not detect any lightning activity below the ISS as well.

From satellite imagery (figure 1), it appears that the southern magnetic field line footpoint is located in the rainbands of a tropical cyclone, named "Joaninha". It is the first time that the detection of a TEB associated to a TGF produced in a cyclone is reported.

Figure 2.a shows the recorded lightcurves for LED and HED, as well as a modeling result. The latter is obtained using what will be referred as the "consensus model", that assumes a source TGF located at the southern magnetic footpoint, at 12 km altitude, with an angular distribution following a Gaussian distribution with $\sigma_\theta = 20^o$ (centered on zenith), and with an energy spectrum $\propto E^{-1} \exp(-E/7.3 \text{ MeV})$ (maximum energy set to 40 MeV). More information about the modeling is presented in the next section. The consensus model gives a very good fit to the data (see figure label). Figure 2.b shows the spectra recorded by the MXGS instrument for LED and HED. There is a total of 168 counts in HED and 307 counts in LED. The error bars are 1-σ ($\approx$68 % interval) assuming Poisson statistics on the count values given by the model. The spectrum shows a strong line at 511 keV, that is expected because the electron beams contains a significant fraction of positrons. The consensus model gives a very good fit to the spectral data as well (see figure label), and a positron to electron ratio of 16.1 %. This value is comparable to previous results (Briggs et al., 2011).

4 Method to constrain the source TGF spectrum

As presented in the introduction, for any considered TGF production scenario, the spectral shape for the TGF is governed by the RREA process that produces high-energy photons through the bremsstrahlung process. A RREA can be more or less developed depending on how many avalanches lengths have been achieved, that depends on the available potential (in the leader and/or background electric field) and the extend of the electric field(s). When the RREA process is close to being fully developed, the resulting TGF photon energy spectrum can be well approximated with equation 1:

$$f(E) \propto E^{-1} \exp\left(-E/\epsilon\right), \text{with } E < E_m \tag{1}$$

Where E is the energy, ϵ is a cut-off energy and E_m is the maximum allowed energy. TGF energy spectra from fully-developed RREA are excepted to have $\epsilon \geq 5$ MeV (Dwyer, 2012; Skeltved et al., 2014; Sarria et al., 2018). Typical TGFs spectra used in the literature have $\epsilon = 6.5$ to 7.3 MeV, with E_m of 30 to 40 MeV. TGF production models based on a propagating lightning leader can, in theory, produce bright TGFs (i.e. detectable from space, therefore with more than 10^{16} photons at source) but that shows a partially developed RREA spectrum. This is because, for these models, typically 10^{12} (or more) energetic electrons are initially provided by the cold runaway mechanism. Leader models with potential drops as low as ≈ 160 MV could potentially produce bright TGFs (see Celestin et al. (2015), table 1). By "potential drop", it is meant the potential difference between the tip of the lightning leader and the ambient potential.

Equation 1 can fit a fully-developed RREA (using $\epsilon \geq 5$ MeV, $E_m = 40$ MeV), as well as partially developped RREA energy spectra resulting from leader models. The leader 300 MV model from Celestin et al. (2015) (figure 3) can be fit by equation 1 with $\epsilon = 4.7$ MeV and $E_m = 30$ MeV as it is close to a fully-developed RREA spectrum. The 160 MV leader model can be fit by equation 1 using $\epsilon = 4.3$ MeV and $E_m = 20$ MeV. In the cases of potential drops of 160 and 300 MV, the initial electron's positions are set at 2 meter and 3.5 meter from the leader tip, respectively, because of the shielding of the electric field (Skeltved et al., 2017). The corresponding effective electric potential drops (i.e. that the energetic electrons can use) are respectively 28 MV, and 53 MV (Celestin et al., 2015).

In addition to the 160 and 300 MV leader spectra, we chose to test spectra with ϵ equal to 6.5 MeV, 7.3 MeV, 8 MeV and 10 MeV (all using $E_m = 40$ MeV). The first two values correspond to values used in the literature (Dwyer et al., 2012; Bowers et al., 2017; Sarria et al., 2018; Xu et al., 2019). After looking at the preliminary results using these two values, we decided to add $\epsilon = 8$ MeV and $\epsilon = 10$ MeV. These last two values were primarily added on an ad hoc basis, but a physical justification is that, in theory, non-uniform electric fields in leader models can also produce TGF spectra harder than typical fully-developed RREA if non-uniform electric fields are involved (Celestin et al., 2012). We decided not to go above ϵ =10 MeV and $E_m = 40$ MeV, since such high energies are irrelevant for TGFs.

To generate a simulated ASIM spectrum, we proceeded to forward modeling of the recorded spectrum, using a two stage simulation. In the first stage, a TGF is started at 12 km altitude, assuming one of the initial energy spectra models, and is propagated to the ISS altitude using the Geant4-based Monte-Carlo model presented in Sarria et al. (2019) and publicly available (see acknowledgments). Energy, 3D-momentum, and times of electrons/positrons reaching the ISS within a radius of 80 km (at ISS altitude) are saved. At the end of this stage, at least 1 million particle records are required for each tested source TGF spectrum model.

In the second stage, the recorded electrons/positrons are used as input of the ASIM mass model to simulate the response of the instrument. It includes a local geomagnetic field, and a rotation of frame of reference (Earth to ISS) is applied. The used mass model includes the ASIM detectors (MXGS, MMIA), the instrument platform, as well as non-negligible surrounding elements (e.g. the Columbus module). The energy deposition on the detectors can be direct, i.e. electrons/positrons hitting directly a CZT or BGO crystal, or indirect. In the indirect case, electrons/positrons emit bremsstrahlung photons by interaction with the surrounding material that hit at least one crystal. Photons can also come from annihilating positrons, with specific energy of 511 keV. For HED, because of the shielding, about 98 % of the energy deposition is due to indirect hits into the BGO crystals. For LED, direct hits are more important: about 72 % of the energy deposition. This explains why the effective area of LED is larger than HED when considering incident electrons/positrons. The effective area is calculated as the geometrical area (≈ 900 cm^2 for HED and ≈ 1024 cm^2 for LED) multiplied by the probability of an incident TEB electron to deposit more than 300 keV into at least one BGO crystal (for HED), or more than 50 keV into at least one CZT pixel (for LED).

At the end of the second stage, a simulation data set in the form of a list of detected time and energy counts is generated. To be able to completely neglect the simulation noise, it is required to have at least 1,000,000 counts on each detector to build each energy spectrum and calculate the effective areas. The final modeled spectra also include a background component build from real background data.

A key feature of performing spectral analysis on the TEB, instead of TGF, is that the energy spectrum of the constituting electrons and positrons above 100 km altitude is only weakly dependent on the following parameters:

- the radial distance between the TEB center and the ISS. The concept of radial is presented more precisely in the supporting information, Figure A.1.
- the beaming and the tilt angles of the source TGF.
- the source altitude of the TGF, if set between 10 and 15 km.

Actually, we found that the spectrum of the source TGF mostly affects the spectrum of the detected TEB. This permit a substantial simplification of the problem as it reduces drastically the number of free parameters to include in the analysis. Since these three points are crucial for this analysis, we provide in the supporting information document more detailed arguments and simulation results supporting those three points. It includes the results of the procedure described below if applied to source TGF altitudes of 10 and 15 km, and various opening angle distribution and tilt angles. The effect of the source TGF altitude is small and does not affect significantly the results presented next (this issue discussed into details in the supporting information, section B). In the following, we fix the model to the "consensus" source altitude to 12 km, the angular distribution to $\sigma = 20^o$, and the tilt angle to 0^o.

The simulated spectra are evaluated with respect to the observation, separately for the LED (50 to 370 keV) and the HED (0.3 to 40 MeV), and with both detectors together. To compare the modeling results to the observation, we use a likelihood analysis, a χ^2 analysis (Eadie et al., 1971; Martin, 1971; Lyons, 1986), and the effective LED/HED area ratio. Note that these three methods are not independent as they used on the same datasets: the list of measured and simulated energy by HED and LED, taken together or separately.

For the likelihood analysis, a value of $-2\,ln(\mathcal{L})$, the Negative Log-Likelihood, is calculated. The model with the lowest value of $-2\,ln(\mathcal{L})$ is considered being the best description of the observation. Models are considered to be also possible if their $-2\,ln(\mathcal{L})$ values have a difference that is less than a threshold value τ. We calculated that $\tau \approx 5$ for a confidence level of about 99%, similar to the one used by Mailyan et al. (2016)

for Fermi-GBM observations. This value assumes that $-2\,ln(\mathcal{L})$ evolves following approximately a normal (a.k.a. Gaussian) distribution with respect to the free parameter(s). In the following, we present the values Δ_{mle}, that are the values of $-2\,ln(\mathcal{L})$ subtracted by the value of $-2\,ln(\mathcal{L})$ for the best model. Therefore the best model has $\Delta_{mle} = 0$ and compatible models have $\Delta_{mle} \leq \tau$. A verification if a given model was found not better than another just because of random fluctuations ("by chance") is also performed.

For completeness, we also provide a reduced χ^2 value, noted χ^2_r. If χ^2_r is below a critical value, the model is considered compatible with the measurement, and above the model is considered incompatible. The Pearson's χ^2 method is affected by choice of binning (i.e. energy intervals chosen to built the spectra). To mitigate this effect, we chose a binning with at least 7 measurement counts on each bin for HED, and at least 10 for LED. These two binnings are used to make the spectra presented in Figure 2.b. Given the used binning, the critical value $\chi^2_{r,c}$ is 1.94 (8 degrees of freedom) for LED, 1.75 for HED (12 degrees of freedom) and 1.57 for the combination of both (20 degrees of freedom).

Compared to the Pearson's χ^2, the maximum likelihood analysis presents the advantage of not relying on a bining of the measurement data: it keeps all its granularity, i.e. no information is lost by binning the measurements. The maximum likelihood analysis is better suited than the χ^2 to estimate which model is the best description of the observation (see, for example, Hauschild and Jentschel (2001))

5 Results and discussion

Table 1 summarizes the results of this study. The models are sorted according the prevalence of high energies (also called "hardness") or, equivalently, by decreasing LED/HED effective area ratio. As indicated in the previous section, three main evaluation criteria are presented: the reduced Pearson's χ^2_r, the maximum likelihood, and the LED/HED effective area ratio.

Concerning the LED spectral fits (table 1), all the models give good fits, using the χ^2_r or the Maximum likelihood analysis. We interpret this as the energy range of 50 keV to 370 keV being too narrow to discriminate between the models. Concerning the HED spectral fits, looking at the χ^2_r values, only the 160 MV leader model is found incompatible. This criterion gives similar conclusions when LED and HED spectra are combined.

The maximum likelihood analysis on the HED spectrum indicates that the best model is for $\epsilon = 8$ MeV. The fit for $\epsilon = 7.3$ MeV is also very close. It indicates that the leader 300 MV model and harder spectra are also possible explanations. If LED and HED spectra are combined, the best model is then $\epsilon = 10$ MeV (but $\epsilon = 8$ MeV is a very close fit here as well), and only models with $\epsilon = 6.5$ MeV or greater are compatible.

Since 307 counts are observed for LED (> 50 keV) and 168 for HED (> 300 keV), the observed ratio is 1.83. Considering that the two count numbers individually follow a Poisson statistic (but the ratio does not), the uncertainty on the ratio is ± 0.35 (95% interval). It implies that, using this criterion, the two leader-based source TGF spectral models (160 MV and 300 MV) are incompatible. The effective area ratio analysis indicates that the models with $\epsilon \geq 6.5$ MeV are compatible. In particular we cannot exclude $\epsilon = 8$ and $\epsilon = 10$ MeV. A similar conclusion is obtained with the maximum likelihood analysis (see last paragraph).

For this event, TGF spectra harder than previously expected are possible. AGILE did report observations of TGF surprisingly hard (up to 100 MeV), but they were later found explainable from instrumental effects (Marisaldi et al., 2019). It does not exclude that the mechanism presented in (Celestin et al., 2012), used first to explain TGF spectra up to 100 MeV, could not be responsible for producing TGFs with a bit harder energy spectra than fully-developed RREA.

The results presented in this article are also only valid for a single event, and it does not imply that leader models with potentials of 300 MV or less could explain other TGF (and TEB) events. It is also possible that because our method relies on the detection of a TEB, we are biased towards a population of strong TGFs, necessitating fully-developed RREAs. TGFs that could originate from non-fully-developed RREAs (leader models) may never (or very rarely) produce a detectable TEB. This question could be addressable in the future, by applying this analysis to more TEB events. We list possibilities of new studies in the next section.

Finally, table 1 also indicates the positron/electron ratio. The model giving the best fit ($\epsilon = 10$ MeV) gives a ratio of 18.3%, and the range of compatible models give a ratio ranging from 15.2% to 18.3%. This range is compatible with estimations from the Fermi space telescope team (Briggs et al., 2011).

6 Conclusions and future work

We reported the observation of a Terrestrial Electron Beam by ASIM on March 24, 2019, originating from the rainbands of the tropical cyclone Johanina. The associated lightning stroke was detected by the GLD360 network (VAISALA) in close temporal association and very close to the ISS's south magnetic field line footpoint. The TEB spectrum was resolved down to 50 keV for the first time, using ASIM's low energy detector. A method to constrain the TGF source energy spectrum based on the TEB detection was presented. It relies on a key reduction of the number of free parameters (altitude, angular distribution, radial distance) possible due to TEB's properties. Comprehensive Monte-Carlo simulations were performed to reproduce the observation, assuming several (energy) spectral shapes of the source TGF. Using three criteria to evaluate the simulation results with respect to the observation (Maximum likelihood, Pearson's χ_r^2 and LED/HED count ratio), we showed that source TGF with, at least, a fully-developed RREA spectrum $\propto E^{-1}\exp(-E/\epsilon)$ (with $\epsilon \geq 6.5$ MeV, $E_m = 40$ MeV) is compatible with the observation. We could not exclude harder models with $\epsilon = 8$ MeV ($E_m = 40$ MeV) and 10 MeV ($E_m = 40$ MeV), that could potentially be explained by non-equilibrium acceleration of energetic electrons in lightning (Celestin et al., 2012).

In the future, we expect that a larger number of events will be processed using the method presented in this article. For ASIM, it will not be possible before several more years of data gathering, since it currently detects about 4 TEB a year, and not all of them present LED data (only turned ON during the night time of the ISS) or enough counts on LED and HED. In principle, the method presented in this article could also be applied/translated to events from the Fermi GBM TGF/TEB catalog (Roberts et al., 2018), that currently contains about 30 TEB events. Fermi GBM has and high energy (BGO-based) detectors that covers an energy range of ≈ 150 keV to ≈ 30 MeV. GBM's NaI detectors could also be used in principle (with an energy range of a few keV to 1 MeV) but no TEB spectrum using it was reported yet. Since TEB events present lower fluxes (counts per second) than TGFs (typically 20 times), it makes the spectral analysis much less challenging than for TGF events. Instrumental effects (dead-time, pile-up), affecting TGF analysis, can be mostly (if not totally) ignored for TEB spectral analysis.

Model	Effective area in cm^2		Effective area ratio	Maximum likelihood analysis result Δ_{mle}			Pearson's χ_r^2			e^+/e^- ratio
	LED	HED		LED	HED	Co.	LED	HED	Co.	
"Leader 160 MV" $\varepsilon = 4.3$ MeV $E_m = 19.2$ MeV	122.0	43.7	2.79	**0**	19.0	22.5	**0.84**	1.97	1.66	10.3 %
"Leader 300 MV" $\varepsilon = 4.7$ MeV $E_m = 32$ MeV	141.5	61.0	2.32	**0**	**3.4**	7.1	**0.88**	**1.04**	**1.31**	13.3 %
$\varepsilon = 6.5$ MeV $E_m = 40$ MeV	156.0	74.4	**2.10**	**0.2**	**0.8**	**3.1**	**0.89**	**0.87**	**1.27**	15.2 %
$\varepsilon = 7.3$ MeV $E_m = 40$ MeV	162.2	80.4	**2.02**	**0.3**	**0.2**	**1.9**	**0.88**	**0.85**	**1.28**	16.1 %
$\varepsilon = 8$ MeV $E_m = 40$ MeV	168.4	85.5	**1.97**	**0.5**	**0**	**1.1**	**0.89**	**0.84**	**1.29**	16.8 %
$\varepsilon = 10$ MeV $E_m = 40$ MeV	177.8	94.7	**1.88**	**0.5**	**1.0**	**0**	**0.90**	**0.83**	**1.30**	18.3 %
Compatibility range	n.a.		1.82±0.35	≤ 5			≤ 1.94	≤ 1.75	≤ 1.57	n.a.

Table 1. Table summarizing the comparison of the tested spectral models with the measurement. Three main criteria are presented: the LED/HED effective area ratio, the maximum likelihood and the Pearson's χ_r^2. "Co." stands for the LED and HED combination. The compatibility range for the different criteria are also indicated. Bold values indicate compatible models for the given criteria (column).

Figure 1. Image from geostationary satellite Meteosat-11 around 00:30 UTC, about 1 minute and 53 seconds before the ASIM trigger. The image comes from the optical band 4 (3.9 μm, 3 km resolution). The tropical cyclone Joaninha can be seen in the south-east part of the picture and extends over a thousand of kilometers. The positions of the International Space Station (ISS), the GLD360 match (V), and the magnetic field line footpoint (M) are indicated. The track of the Earth's magnetic field line (blue dashed line) and of ISS trajectory (green dashed line) are also showed. Point V is very close to M in both location ($\Delta r = 4.82$ km) and time ($\Delta t = 1.44$ ms), and is located in the north-western rainbands of the cyclone.

7 Acknowledgments

The data presented in this article is available in the following Zenodo repository: `https://doi.org/10.5281/zenodo.4264459`

This work was supported by the European Research Council under the European Union's Seventh Framework Program (FP7/2007-2013)/ERC grant agreement n. 320839 and the Research Council of Norway under contract 223252/F50 (CoE). ASIM is a mission of ESA's SciSpace Programme for scientific utilization of the ISS and non-ISS space exploration platforms and space environment analogues. This study has received funding from the European Union's Horizon 2020 research and innovation programme under the Marie Sklodowska-Curie grant agreement SAINT 722337. ASIM was funded through the ESA ELIPS program, through contracts with TERMA and Danish Technical University (DTU) in Denmark, University of Bergen (UB) in Norway and University of Valencia (UV) in Spain. Additional funding was supported by the ESA PRODEX contracts PEA 4000105639 and 4000111397 to DTU and ESA PRODEX contract 4000102100 and by Norwegian Research Council to UB. The ASIM Science Data Centre (ASDC) at DTU is supported by PRODEX contract PEA 4000115884 and by PRODEX contract PEA4000123438 at UB. The ASIM Science Data Centre and data analysis activities at the UV are supported by the MINECO Research Grants ESP2015- 69909-C5-1-R and ESP2017-86263-C4-1-R.

We thank Vaisala Inc. for access to the GLD360 data. For more information, see `https://www.GLD360.com/en/products/systems/lightning129detection-networks`.

We acknowledge EUMETSAT for making accessible images from the Meteosat-11 geostationary satellite and the MCFETCH service (`https://mcfetch.ssec.wisc.edu/`) from the Satellite Data Services (SDS) group, at the University of Wisconsin-Madison Space Science and Engineering Center (SSEC), that is responsible for the access, maintenance, and distribution of real-time and archive weather satellite data.

The simulations were performed on resources provided by UNINETT Sigma2 - the National Infrastructure for High Performance Computing and Data Storage in Norway, under project no. NN9526K.

The Geant4-based model for Terrestrial Gamma-ray Flash (TGF) and associated electrons and positrons propagation in Earth atmosphere and environment (magnetic

field) is available in the following GitHub repository: `https://github.com/DavidSarria89/TGF-Propagation-Geant4`, or the DOI: `https://doi.org/10.5281/zenodo.2597039`.

References

Babich, L. P., Donskoy, E. N., Kutsyk, I. M., & Roussel-Dupré, R. A. (2005). The feedback mechanism of runaway air breakdown. *Geophysical Research Letters*, *32*(9). doi: 10.1029/2004GL021744

Bowers, G. S., Smith, D. M., Martinez-McKinney, G. F., Kamogawa, M., Cummer, S. A., Dwyer, J. R., ... Kawasaki, Z. (2017). Gamma Ray Signatures of Neutrons From a Terrestrial Gamma Ray Flash. *Geophysical Research Letters*, *44*(19). doi: 10.1002/2017GL075071

Briggs, M. S., Connaughton, V., Wilson-Hodge, C., Preece, R. D., Fishman, G. J., Kippen, R. M., ... Smith, D. M. (2011). Electron-positron beams from terrestrial lightning observed with Fermi GBM. *Geophysical Research Letters*, *38*, L02808. doi: 10.1029/2010GL046259

Briggs, M. S., Fishman, G. J., Connaughton, V., Bhat, P. N., Paciesas, W. S., Preece, R. D., ... Chekhtman, A. (2010). First results on terrestrial gamma ray flashes from the Fermi Gamma-ray Burst Monitor. *Journal of Geophysical Research (Space Physics)*, *115*, A07323. doi: 10.1029/2009JA015242

Celestin, S., & Pasko, V. P. (2011). Energy and fluxes of thermal runaway electrons produced by exponential growth of streamers during the stepping of lightning leaders and in transient luminous events. *Journal of Geophysical Research (Space Physics)*, *116*, A03315. doi: 10.1029/2010JA016260

Celestin, S., Xu, W., & Pasko, V. P. (2012). Terrestrial gamma ray flashes with energies up to 100 MeV produced by nonequilibrium acceleration of electrons in lightning. *Journal of Geophysical Research (Space Physics)*, *117*(A5). doi: 10.1029/2012JA017535

Celestin, S., Xu, W., & Pasko, V. P. (2015). Variability in fluence and spectrum of high-energy photon bursts produced by lightning leaders. *Journal of Geophysical Research (Space Physics)*, *120*(12), 10,712–10,723. doi: 10.1002/2015JA021410

Chanrion, O., Bonaventura, Z., Çinar, D., Bourdon, A., & Neubert, T. (2014). Runaway electrons from a 'beam-bulk' model of streamer: application to TGFs.

Environmental Research Letters, *9*(5), 055003. doi: 10.1088/1748-9326/9/5/055003

Chanrion, O., Neubert, T., Lundgaard Rasmussen, I., Stoltze, C., Tcherniak, D., Jessen, N. C., … Lorenzen, M. (2019). The Modular Multispectral Imaging Array (MMIA) of the ASIM Payload on the International Space Station. *ßr*, *215*, 28. doi: 10.1007/s11214-019-0593-y

Cohen, M. B., Inan, U. S., Said, R. K., Briggs, M. S., Fishman, G. J., Connaughton, V., & Cummer, S. A. (2010). A lightning discharge producing a beam of relativistic electrons into space. *Geophysical Research Letters*, *37*(18), L18806. doi: 10.1029/2010GL044481

Dwyer, J. R. (2008). Source mechanisms of terrestrial gamma-ray flashes. *Journal of Geophysical Research (Atmospheres)*, *113*(D10), D10103. doi: 10.1029/2007JD009248

Dwyer, J. R. (2012). The relativistic feedback discharge model of terrestrial gamma ray flashes. *Journal of Geophysical Research (Space Physics)*, *117*(A2), A02308. doi: 10.1029/2011JA017160

Dwyer, J. R., Grefenstette, B. W., & Smith, D. M. (2008). High-energy electron beams launched into space by thunderstorms. *Geophysical Research Letters*, *35*, L02815. doi: 10.1029/2007GL032430

Dwyer, J. R., Rassoul, H. K., Al-Dayeh, M., Caraway, L., Chrest, A., Wright, B., … others (2005). X-ray bursts associated with leader steps in cloud-to-ground lightning. *Geophysical Research Letters*, *32*(1).

Dwyer, J. R., Rassoul, H. K., Al-Dayeh, M., Caraway, L., Wright, B., Chrest, A., … others (2004). Measurements of X-ray emission from rocket-triggered lightning. *Geophysical research letters*, *31*(5).

Dwyer, J. R., Schaal, M., Rassoul, H. K., Uman, M. A., Jordan, D. M., & Hill, D. (2011). High-speed X-ray images of triggered lightning dart leaders. *Journal of Geophysical Research:Atmospheres*, *116*(D15), D20208. doi: 10.1029/2011JD015973

Dwyer, J. R., Smith, D. M., Cummer, S. A., ., ., ., … . (2012). High-Energy Atmospheric Physics: Terrestrial Gamma-Ray Flashes and Related Phenomena. *Space Science Reviews*, *173*(1-4), 133–196. doi: 10.1007/s11214-012-9894-0

Dwyer, J. R., Uman, M. A., Rassoul, H. K., Al-Dayeh, M., Caraway, L., Jerauld, J.,

… Wright, B. (2003). Energetic Radiation Produced During Rocket-Triggered Lightning. *Science*, *299*, 694–697. doi: 10.1126/science.1078940

Eadie, W. T., Drijard, D., James, F. E., Roos, M., & Sadoulet, B. (1971). *Statistical methods in experimental physics.* Amsterdam: North-Holland. Retrieved from https://cds.cern.ch/record/100342

Fishman, G. J., Bhat, P. N., Mallozzi, R., Horack, J. M., Koshut, T., Kouveliotou, C., … Christian, H. J. (1994). Discovery of Intense Gamma-Ray Flashes of Atmospheric Origin. *Science*, *264*(5163), 1313–1316. doi: 10.1126/science.264.5163.1313

Gjesteland, T. (2012). *Properties of Terrestrial Gamma ray Flashes. Modelling and Analysis of BATSE and RHESSI data* (PhD Thesis, The University of Bergen). Retrieved from http://bora.uib.no/handle/1956/6203

Gurevich, A. V. (1961). On the theory of runaway electrons. *Sov. Phys. JETP*, *12*(5), 904–912.

Gurevich, A. V., Milikh, G. M., & Roussel-Dupre, R. (1992). Runaway electron mechanism of air breakdown and preconditioning during a thunderstorm. *Physics Letters A*, *165*(5-6), 463–468.

Hauschild, T., & Jentschel, M. (2001). Comparison of maximum likelihood estimation and chi-square statistics applied to counting experiments. *Nuclear Instruments and Methods in Physics Research Section A: Accelerators, Spectrometers, Detectors and Associated Equipment*, *457*(1), 384 – 401. Retrieved from http://www.sciencedirect.com/science/article/pii/S0168900200007567 doi: 10.1016/S0168-9002(00)00756-7

Kohn, C., & Ebert, U. (2015). Calculation of beams of positrons, neutrons, and protons associated with terrestrial gamma ray flashes. *Journal of Geophysical Research:Atmospheres*, *120*(4), 1620–1635. doi: 10.1002/2014JD022229

Lindanger, A., Marisaldi, M., Maiorana, C., Sarria, D., Albrechtsen, K., Østgaard, N., … Verrecchia, F. (2020). The 3rd AGILE Terrestrial Gamma Ray Flash Catalog. Part I: Association to Lightning Sferics. *Journal of Geophysical Research:Atmospheres*, *125*(11), e2019JD031985. doi: 10.1029/2019JD031985

Lyons, L. (1986). *STATISTICS FOR NUCLEAR AND PARTICLE PHYSICISTS.*

Mailyan, B. G., Briggs, M. S., Cramer, E. S., Fitzpatrick, G., Roberts, O. J., Stanbro, M., … Dwyer, J. R. (2016). The spectroscopy of individual terrestrial gamma-ray flashes: Constraining the source properties. *Journal of Geophysical Research (Space Physics)*, *121*(A10), 11. doi: 10.1002/2016JA022702

Mailyan, B. G., Xu, W., Celestin, S., Briggs, M. S., Dwyer, J. R., Cramer, E. S., … Stanbro, M. (2019). Analysis of Individual Terrestrial Gamma-Ray Flashes With Lightning Leader Models and Fermi Gamma-Ray Burst Monitor Data. *Journal of Geophysical Research (Space Physics)*, *124*(8), 7170–7183. Retrieved from https://agupubs.onlinelibrary.wiley.com/doi/abs/10.1029/2019JA026912 doi: 10.1029/2019JA026912

Marisaldi, M., Fuschino, F., Tavani, M., Dietrich, S., Price, C., Galli, M., … Vercellone, S. (2014). Properties of terrestrial gamma ray flashes detected by AGILE MCAL below 30 MeV. *Journal of Geophysical Research (Space Physics)*, *119*, 1337–1355. doi: 10.1002/2013JA019301

Marisaldi, M., Galli, M., Labanti, C., Østgaard, N., Sarria, D., Cummer, S. A., … Verrecchia, F. (2019). On the High-Energy Spectral Component and Fine Time Structure of Terrestrial Gamma Ray Flashes. *Journal of Geophysical Research:Atmospheres*, *124*(14), 7484–7497. Retrieved 2021-01-22, from https://onlinelibrary.wiley.com/doi/abs/10.1029/2019JD030554 doi: 10.1029/2019JD030554

Martin, B. R. (1971). *Statistics for physicists [by] B. R. Martin.* Academic Press London, New York.

Moss, G. D., Pasko, V. P., Liu, N., & Veronis, G. (2006). Monte Carlo model for analysis of thermal runaway electrons in streamer tips in transient luminous events and streamer zones of lightning leaders. *Journal of Geophysical Research (Space Physics)*, *111*, 2307. doi: 10.1029/2005JA011350

Neubert, T., Østgaard, N., Reglero, V., Blanc, E., Chanrion, O., Oxborrow, C. A., … Bhanderi, D. D. V. (2019). The ASIM Mission on the International Space Station. *Space Science Reviews*, *215*(2), 26. Retrieved 2021-01-22, from http://link.springer.com/10.1007/s11214-019-0592-z doi: 10.1007/s11214-019-0592-z

Neubert, T., Østgaard, N., Reglero, V., Chanrion, O., Heumesser, M., Dimitriadou, K., … Eyles, C. J. (2019). A terrestrial gamma-ray flash and ionospheric ultraviolet emissions powered by lightning. *Science*, eaax3872. Retrieved 2021-01-20, from https://www.sciencemag.org/lookup/doi/10.1126/

science.aax3872 doi: 10.1126/science.aax3872

Østgaard, N., Balling, J. E., Bjørnsen, T., Brauer, P., Budtz-Jørgensen, C., Bujwan, W., ... Yang, S. (2019). The Modular X- and Gamma-Ray Sensor (MXGS) of the ASIM Payload on the International Space Station. *Space Science Reviews*, *215*, 23. doi: 10.1007/s11214-018-0573-7

Østgaard, N., Neubert, T., Reglero, V., Ullaland, K., Yang, S., Genov, G., ... Al-nussirat, S. (2019). First 10 Months of TGF Observations by ASIM. *Journal of Geophysical Research:Atmospheres*, *124*(24), 14024–14036. Retrieved 2021-01-20, from https://onlinelibrary.wiley.com/doi/10.1029/2019JD031214 doi: 10.1029/2019JD031214

Roberts, O. J., Fitzpatrick, G., Stanbro, M., McBreen, S., Briggs, M. S., Holzworth, R. H., ... Mailyan, B. G. (2018). The First Fermi-GBM Terrestrial Gamma Ray Flash Catalog. *Journal of Geophysical Research (Space Physics)*, *123*, 4381–4401. doi: 10.1029/2017JA024837

Rudlosky, S. D., Peterson, M. J., & Kahn, D. T. (2017). GLD360 Performance Relative to TRMM LIS. *Journal of Atmospheric and Oceanic Technology*, *34*(6), 1307 – 1322. doi: 10.1175/JTECH-D-16-0243.1

Sarria, D., Blelly, P.-L., & Forme, F. (2015). MC-PEPTITA: A Monte Carlo model for Photon, Electron and Positron Tracking In Terrestrial Atmosphere—Application for a terrestrial gamma ray flash. *Journal of Geophysical Research (Space Physics)*, *120*(5), 3970–3986. Retrieved from https://agupubs.onlinelibrary.wiley.com/doi/abs/10.1002/2014JA020695 doi: 10.1002/2014JA020695

Sarria, D., Kochkin, P. O., Østgaard, N., Lehtinen, N. G., Mezentsev, A., Marisaldi, M., ... Eyles, C. (2019). The First Terrestrial Electron Beam Observed by the Atmosphere-Space Interactions Monitor. *Journal of Geophysical Research (Space Physics)*, *124*(12), 10,497–10,511. doi: 10.1029/2019JA027071

Sarria, D., Rutjes, C., Diniz, G., Luque, A., Ihaddadene, K. M. A., Dwyer, J. R., ... Ebert, U. (2018). Evaluation of Monte Carlo tools for high-energy atmospheric physics II: relativistic runaway electron avalanches. *Geoscientific Model Development*, *11*, 4515–4535. doi: 10.5194/gmd-11-4515-2018

Skeltved, A. B., Østgaard, N., Carlson, B. E., Gjesteland, T., & Celestin, S. (2014). Modeling the relativistic runaway electron avalanche and the feedback mechanism with GEANT4. *Journal of Geophysical Research (Space Physics)*, *119*, 9174–9191. doi: 10.1002/2014JA020504

Skeltved, A. B., Østgaard, N., Mezentsev, A., Lehtinen, N. G., & Carlson, B. E. (2017). Constraints to do realistic modeling of the electric field ahead of the tip of a lightning leader. *Journal of Geophysical Research:Atmospheres*, *122*(15), 8120–8134. Retrieved from `https://agupubs.onlinelibrary.wiley.com/doi/abs/10.1002/2016JD026206` doi: 10.1002/2016JD026206

Smith, D. M., Grefenstette, B. W., Splitt, M., Lazarus, S. M., Rassoul, H. K., Coleman, L. M., ... Takahashi, Y. (2006). The Anomalous Terrestrial Gamma-ray Flash of 17 January 2004. *AGU Fall Meeting Abstracts*, AE31A–1040.

Smith, D. M., Lopez, L. I., Lin, R. P., & Barrington-Leigh, C. P. (2005). Terrestrial Gamma-Ray Flashes Observed up to 20 MeV. *Science*, *307*, 1085–1088. doi: 10.1126/science.1107466

Stanbro, M., Briggs, M. S., Roberts, O. J., Cramer, E., Dwyer, J. R., Holzworth, R., ... Xiong, S. L. (2019). A Fermi Gamma-Ray Burst Monitor Event Observed as a Terrestrial Gamma-Ray Flash and Terrestrial Electron Beam. *Journal of Geophysical Research (Space Physics)*, *124*(12), 10580–10591. Retrieved from `https://agupubs.onlinelibrary.wiley.com/doi/abs/10.1029/2019JA026749` doi: 10.1029/2019JA026749

Ursi, A., Guidorzi, C., Marisaldi, M., Sarria, D., & Frontera, F. (2017). Terrestrial gamma-ray flashes in the BeppoSAX data archive. *Journal of Atmospheric and Solar-Terrestrial Physics*, *156*, 50–56. doi: 10.1016/j.jastp.2017.02.014

Wilson, C. T. R. (1924). The electric field of a thundercloud and some of its effects. *Proceedings of the Physical Society of London*, *37*, 32D–37D.

Xu, W., Celestin, S., Pasko, V. P., & Marshall, R. A. (2019). Compton Scattering Effects on the Spectral and Temporal Properties of Terrestrial Gamma-Ray Flashes. *Journal of Geophysical Research (Space Physics)*, *124*(8), 7220–7230. Retrieved from `https://agupubs.onlinelibrary.wiley.com/doi/abs/10.1029/2019JA026941` doi: 10.1029/2019JA026941

Constraining spectral models of a terrestrial gamma-ray flash from a terrestrial electron beam observation by the Atmosphere-Space Interactions Monitor

D. Sarria[1], N. Østgaard[1], P. Kochkin[1], N. Lehtinen[1], A. Mezentsev[1], M. Marisaldi[1], A. Lindanger[1], C. Maiorana[1], B. E. Carlson[1,2], T. Neubert[3], V. Reglero[4], K. Ullaland[1], S.Yang[1], G. Genov[1], B. H. Qureshi[1], C. Budtz-Jørgensen[3], I. Kuvvetli[3], F. Christiansen[3], O. Chanrion[3], J. Navarro-González[4], P. Connel[4], C. Eyles[4]

[1]Birkeland Centre for Space Science, University of Bergen, Bergen, Norway
[2]Carthage College, Kenosha, Wisconsin, United States
[3]National Space Institute, Technical University of Denmark, Lyngby, Denmark
[4]University of Valencia, Valencia, Spain

Key Points:

- Observation of a Terrestrial Electron Beam with a spectrum resolved down to 50 keV
- A method to constrain the energy spectrum of the source Terrestrial Gamma-ray Flash based on the detection of the associated TEB is presented
- Only TGFs originating from fully-developed RREA models can explain the observation

Corresponding author: D. Sarria, `david.sarria@uib.no`

Abstract

Terrestrial Gamma-ray Flashes (TGFs) are short flashes of high energy photons, produced by thunderstorms. When interacting with the atmosphere, they produce relativistic electrons and positrons, and a part gets bounded to geomagnetic field lines and travels large distances in space. This phenomenon is called a Terrestrial Electron Beam (TEB). The Atmosphere-Space Interactions Monitor (ASIM) mounted on-board the International Space Station detected a new TEB event on March 24, 2019, originating from the tropical cyclone Johanina. Using ASIM's low energy detector, the TEB energy spectrum is resolved down to 50 keV. We provide a method to constrain the TGF source spectrum based on the detected TEB spectrum. Applied to this event, it shows that only fully developed RREA spectra are compatible with the observation. More specifically, assuming a TGF spectrum $\propto E^{-1}\exp(-E/\epsilon)$, the compatible models have $\epsilon \geq 6.5$ MeV (E is the photon energy and ϵ is the cut-off energy). We could not exclude models with ϵ of 8 and 10 MeV.

Plain Language Summary

Terrestrial Gamma-ray Flashes (TGF), originating from thunderstorms, are the highest energy natural particle acceleration phenomena occurring on Earth. The production mechanism of TGFs is not very well understood. When interacting with the atmosphere, TGFs produce secondary electrons and positrons, and a part gets bounded to Earth's magnetic field lines, and travels large distances in space. They can be detected by instruments on-board satellites located at the right place (in a window of about 40 km) at the right time (in a window of a few milliseconds). This phenomenon is called a Terrestrial Electron Beam (TEB). By detecting the TEB, we can retrieve information about the TGF that produced it. In this article we present the first TEB originating from a tropical cyclone, and with the lowest energies ever recorded (down to 50 keV). We also provide a method to infer properties of the energy distribution of the TGF (producing the TEB) based on the energy spectrum of the TEB. Applied to this event, it shows that only TGF energy spectra among the most energetic that were proposed are compatible, and we cannot exclude even more energetic events.

1 Introduction

Terrestrial Gamma-ray Flashes (TGFs) are short bursts of high energy ($<$ 40 MeV) photons, produced during thunderstorms. A review of TGFs theory and observations is presented by Dwyer et al. (2012). TGFs were first detected using the BATSE experiment on-board the CGRO spacecraft (Fishman et al., 1994). Later, TGFs were recorded by the satellites RHESSI (Smith et al., 2005), AGILE (Marisaldi et al., 2014), Fermi (Briggs et al., 2010; Roberts et al., 2018), BeppoSAX (Ursi et al., 2017) and the Atmosphere-Space Interactions Monitor (ASIM) (Neubert, Østgaard, Reglero, Blanc, et al., 2019). ASIM was successfully launched and docked to the International Space Station in April 2018, and started science operations since June 2018. The first results from ASIM were presented by Østgaard, Neubert, et al. (2019); Sarria et al. (2019); Neubert, Østgaard, Reglero, Chanrion, et al. (2019).

When referring to "electrons beams" in the context of TGFs, one can think of two different objects. The first is associated with the production process of the TGF. This production process takes place, at least for TGF detectable from space, between $\approx$10 and $\approx$15 km altitude. This first type of "electron beam" consists of the Relativistic Runaway Electron Avalanche (RREA) producing the TGF's high energy photons. This RREA is not detectable from space since it is is impossible for it to go through the atmosphere layer. The second type of "electron beam" is called "terrestrial electron beam" (TEB) and is produced higher in the atmosphere by the TGF's photons, though the processes of Compton scattering and electron-positron pair production. Since electron-positron pair production is involved, TEBs are composed of a fraction of positrons, typically 10 % to 30 % (see Briggs et al. (2011), table 1). A TEB is bound ("beamed") around the magnetic field line intercepting the source TGF's geographical location (Dwyer et al., 2008; Cohen et al., 2010; Sarria et al., 2015). Most electrons and positrons forming TEBs are produced above 40 km altitude, where the air collision frequency of the electrons (and positrons) is comparable to their gyration frequency around geomagnetic field lines. TEBs propagate in space and travel large distances in the magnetosphere. TEBs were first reported from measurements of the CGRO spacecraft (Dwyer et al., 2008). Later, they were detected by Fermi (Briggs et al., 2011; Stanbro et al., 2019), BeppoSAX (Ursi et al., 2017), AGILE (Lindanger et al., 2020) and ASIM (Sarria et al., 2019). RHESSI probably detected one or two TEB event(s), but it has not been 100% confirmed yet (Smith et al., 2006; Gjesteland, 2012). In general, TEBs are detected much less often than TGFs (e.g.

Fermi has a few thousand TGFs and about 30 TEBs) because the detector must be located inside a narrow window of less than a few tens of kilometers along the right geomagnetic field line (intercepting the TGF source position), and they last for only a few milliseconds.

One of the reasons of studing TEBs is to retrieve information about the TGFs that produced them. Briggs et al. (2011) constrained the positron fraction to be between 10 and 34%, based on 3 events. Positrons fractions are linked to the spectral shape of the source TGF, as photons with harder specturms will do more pair production. In Sarria et al. (2019), the beaming of the source TGF could be constrained between about 30^o and 42^o (half angle, isotropic within a cone). Another reason to study TEBs is that they may have an impact on the inner Van Allen radiation belt, that has not been quantified yet (to our knowledge). Even if it is an important question, it is not the subject of the present paper.

One of the most important question regarding TGFs is their production mechanism. Two main models are proposed to explain the production of TGFs, and in both, the TGF's photons are produced by high energy electrons through the bremsstrahlung process. These high energy electrons form a Relativistic Runaway Electron Avalanche (RREA) (Wilson, 1924; Gurevich et al., 1992). In the first model, a large scale electric field within thunderclouds is considered. This requires the presence of initial high energy seed electrons, that may be provided by cosmic-ray secondaries or background radiation. The background electric field is strong enough to produce RREA avalanches, but the RREA mechanism alone is not enough to produce bright enough TGFs (i.e. detectable from space, therefore with more than 10^{16} photons between 50 keV and 40 MeV at source), and a x-ray and positron feedback mechanism is required (the "relativistic feedback"); only possible if large potentials are available (Dwyer et al., 2003; Babich et al., 2005; Dwyer, 2012; Skeltved et al., 2014). This mechanism will produce a discharge of the thundercloud, that is of different nature than usual lightning discharges. The resulting high-energy photon spectrum given by this model is a so-called "fully-developed" RREA. The development of a RREA process can be characterized by the number of avalanche lengths that were achieved (that depends on the extend and magnitude of the available electric potential). The energy spectrum of the electrons converges to a standard shape ($\approx \exp(-E/7.3\text{MeV})$), which is fully obtained with six or more avalanche lengths, even if the total number of electrons keeps exponentially increasing with the number of avalanche lengths. Another variant of this model uses a lightning leader to push the background (large scale) field above the threshold to trigger the relativistic feedback mechanism (Skeltved et al., 2017).

The second model of TGF production requires a propagating lightning leader. It is sometimes referred as the "leader-streamer" model. It considers that initial seed electrons are produced by the cold runaway mechanism (Gurevich, 1961), happening in the streamer phase or in the leader phase (Moss et al., 2006; Dwyer, 2008; Celestin & Pasko, 2011; Chanrion et al., 2014; Kohn & Ebert, 2015). These energetic seed electrons follow a specific distribution and a fraction of them are then accelerated and multiplied by a larger scale electric field, producing a RREA. The larger scale electric field can be the field induced by the leader and/or a large scale (background) field in the thunderstorm. In principle, leader-based TGF production models do not exclude the possibility of relativistic feedback, that could be more or less important (Skeltved et al., 2017). A parameter that impacts the energy spectrum of emitted photons the most is the potential drop in the leader tip region that is available for the acceleration of energetic electrons. Resulting TGF energy spectra for several leader potential drops are presented in Celestin et al. (2015), figure 3. They actually correspond to a more or less developed RREA process. Celestin et al. (2012) also showed that energy spectra harder than this characteristic fully-developed RREA spectrum could be achieved by involving non-equilibrium acceleration of electrons. One significant advantage of leader-based TGF models is that they propose an unified approach to explain TGF's X/gamma-ray production, as well as x-ray (i.e. softer) emissions from lightning propagating leaders, that were observed from ground, balloons and aircraft (Dwyer et al., 2003, 2004, 2005, 2011). Mailyan et al. (2019) presented the first study that confronted leader models to TGFs recorded by the Fermi space telescope, with tested potential drops $\leq$ 200 MV. They found that lightning leader models with potentials of 200 MV and tilted beams gave the best fit to the data in most of the analyzed TGF events. However, the range of compatible models is found to be quite wide.

In this article, we report the second TEB event detected by ASIM on 24 March 2019. Compared to the previous event (presented in Sarria et al. (2019)), data from the two detectors are available: the pixelated Low-Energy detector (50-400 keV) and the High Energy Detector (300 keV-30 MeV), that permits an unprecedented spectral analysis of a TEB event. In section 2, we present the instruments that were used. In section 3 we present the event. In section 4 we present the methods and models we use for the spectral analysis. In section 5 we show the results of the analysis. We conclude in section 6.

2 Instruments

The ASIM payload (Neubert, Østgaard, Reglero, Blanc, et al., 2019) consists of two main instruments, the Modular X- and Gamma-ray Sensor (MXGS) (Østgaard, Balling, et al., 2019) and the Modular Multi-spectral Imaging Array (MMIA) (Chanrion et al., 2019). ASIM is mounted on the International Space Station (ISS) orbiting the Earth at about 400 kilometers altitude with an inclination of 51.6^o. MXGS consists of two detectors for detecting X- and gamma-rays. The MXGS Low-Energy Detector (LED) is layer of 16384 pixels of Cadmium-Zink-Telluride (CZT) detector crystals, sensitive to photons with energies from 50 keV to about 400 keV. The MXGS High Energy Detector (HED) comprises 12 Bismuth-Germanium-Oxide (BGO) detector modules coupled to photomultiplier tubes (PMT), sensitive in the energy range of 300 keV to about 40 MeV.

GLD360 (VAISALA) is a network of ground-based lightning sensors (1 kHz-350 kHz) detecting both Cloud-to-Groung and Intra-Cloud lightning. The GLD360 sensors use a combination of magnetic direction finding and time-of-arrival calculations (from 4 stations or more) to geolocate the lightning source (see acknowledgments for more details). The typical uncertainty on location is about 2.5 km and it can vary a lot with geographical location (Rudlosky et al., 2017).

We also present data provided by the Meteosat-11 geostationary satellite, that provides regular scans of cloud coverage at several wavelengths (used data comes from band 4, at 3.9 μm, with a 3 km spatial resolution). See acknowledgments for more information.

3 Observation

Figure 1 shows a map of the event together with Satellite imagery that was provided by the geostationary satellite Meteosat-11. The ASIM trigger UTC time is 2019-Mar-24 00:31:53.135444 and the ISS was located at latitude of $\phi = 0.157^o$, longitude of $\lambda = 55.301^o$ and altitude of $h = 408.6$ km, that is above the Indian ocean, close to Madagascar. The ASIM clock has a -20 to 30 ms absolute timing uncertainty with respect to GPS UTC time. A VAISALA (GLD360) discharge event with a UTC time of

2019-03-24 00:31:53.134000 ($\Delta t = 1.44$ ms) was found very close to the southern magnetic line footpoint (at 45 km altitude) intercepting the ISS position : [$\phi_{GLD360} = -7.049^o$, $\lambda_{GLD360} = 55.912^o$] and [$\phi_{mag,s} = -7.007^o$, $\lambda_{mag,s} = 55.923^o$] that gives $\Delta r = 4.82$ km. Note that the GLD360 location uncertainty can be up to 20 km for this event, and the uncertainty in the ISS position is of the same order. The northern magnetic field line footpoint is located at [$\phi_{mag,n} = 20.524^o$, $\lambda_{mag,n} = 55.099^o$], but no lightning activity was observed close to it. No lightning activity was detected by GLD360 below the ISS, within 540 km and ± 1 second around the trigger time. The MMIA photometers did not detect any lightning activity below the ISS as well.

From satellite imagery (figure 1), it appears that the southern magnetic field line footpoint is located in the rainbands of a tropical cyclone, named "Joaninha". It is the first time that the detection of a TEB associated to a TGF produced in a cyclone is reported.

Figure 2.a shows the recorded lightcurves for LED and HED, as well as a modeling result. The latter is obtained using what will be referred as the "consensus model", that assumes a source TGF located at the southern magnetic footpoint, at 12 km altitude, with an angular distribution following a Gaussian distribution with $\sigma_\theta = 20^o$ (centered on zenith), and with an energy spectrum $\propto E^{-1} \exp(-E/7.3 \text{ MeV})$ (maximum energy set to 40 MeV). More information about the modeling is presented in the next section. The consensus model gives a very good fit to the data (see figure label). Figure 2.b shows the spectra recorded by the MXGS instrument for LED and HED. There is a total of 168 counts in HED and 307 counts in LED. The error bars are 1-σ ($\approx$68 % interval) assuming Poisson statistics on the count values given by the model. The spectrum shows a strong line at 511 keV, that is expected because the electron beams contains a significant fraction of positrons. The consensus model gives a very good fit to the spectral data as well (see figure label), and a positron to electron ratio of 16.1 %. This value is comparable to previous results (Briggs et al., 2011).

4 Method to constrain the source TGF spectrum

As presented in the introduction, for any considered TGF production scenario, the spectral shape for the TGF is governed by the RREA process that produces high-energy photons through the bremsstrahlung process. A RREA can be more or less developed depending on how many avalanches lengths have been achieved, that depends on the available potential (in the leader and/or background electric field) and the extend of the electric field(s). When the RREA process is close to being fully developed, the resulting TGF photon energy spectrum can be well approximated with equation 1:

$$f(E) \propto E^{-1} \exp\left(-E/\epsilon\right), \text{with } E < E_m \tag{1}$$

Where E is the energy, ϵ is a cut-off energy and E_m is the maximum allowed energy. TGF energy spectra from fully-developed RREA are excepted to have $\epsilon \geq 5$ MeV (Dwyer, 2012; Skeltved et al., 2014; Sarria et al., 2018). Typical TGFs spectra used in the literature have $\epsilon = 6.5$ to 7.3 MeV, with E_m of 30 to 40 MeV. TGF production models based on a propagating lightning leader can, in theory, produce bright TGFs (i.e. detectable from space, therefore with more than 10^{16} photons at source) but that shows a partially developed RREA spectrum. This is because, for these models, typically 10^{12} (or more) energetic electrons are initially provided by the cold runaway mechanism. Leader models with potential drops as low as ≈ 160 MV could potentially produce bright TGFs (see Celestin et al. (2015), table 1). By "potential drop", it is meant the potential difference between the tip of the lightning leader and the ambient potential.

Equation 1 can fit a fully-developed RREA (using $\epsilon \geq 5$ MeV, $E_m = 40$ MeV), as well as partially developped RREA energy spectra resulting from leader models. The leader 300 MV model from Celestin et al. (2015) (figure 3) can be fit by equation 1 with $\epsilon = 4.7$ MeV and $E_m = 30$ MeV as it is close to a fully-developed RREA spectrum. The 160 MV leader model can be fit by equation 1 using $\epsilon = 4.3$ MeV and $E_m = 20$ MeV. In the cases of potential drops of 160 and 300 MV, the initial electron's positions are set at 2 meter and 3.5 meter from the leader tip, respectively, because of the shielding of the electric field (Skeltved et al., 2017). The corresponding effective electric potential drops (i.e. that the energetic electrons can use) are respectively 28 MV, and 53 MV (Celestin et al., 2015).

In addition to the 160 and 300 MV leader spectra, we chose to test spectra with ϵ equal to 6.5 MeV, 7.3 MeV, 8 MeV and 10 MeV (all using $E_m = 40$ MeV). The first two values correspond to values used in the literature (Dwyer et al., 2012; Bowers et al., 2017; Sarria et al., 2018; Xu et al., 2019). After looking at the preliminary results using these two values, we decided to add $\epsilon = 8$ MeV and $\epsilon = 10$ MeV. These last two values were primarily added on an ad hoc basis, but a physical justification is that, in theory, non-uniform electric fields in leader models can also produce TGF spectra harder than typical fully-developed RREA if non-uniform electric fields are involved (Celestin et al., 2012). We decided not to go above ϵ =10 MeV and $E_m = 40$ MeV, since such high energies are irrelevant for TGFs.

To generate a simulated ASIM spectrum, we proceeded to forward modeling of the recorded spectrum, using a two stage simulation. In the first stage, a TGF is started at 12 km altitude, assuming one of the initial energy spectra models, and is propagated to the ISS altitude using the Geant4-based Monte-Carlo model presented in Sarria et al. (2019) and publicly available (see acknowledgments). Energy, 3D-momentum, and times of electrons/positrons reaching the ISS within a radius of 80 km (at ISS altitude) are saved. At the end of this stage, at least 1 million particle records are required for each tested source TGF spectrum model.

In the second stage, the recorded electrons/positrons are used as input of the ASIM mass model to simulate the response of the instrument. It includes a local geomagnetic field, and a rotation of frame of reference (Earth to ISS) is applied. The used mass model includes the ASIM detectors (MXGS, MMIA), the instrument platform, as well as non-negligible surrounding elements (e.g. the Columbus module). The energy deposition on the detectors can be direct, i.e. electrons/positrons hitting directly a CZT or BGO crystal, or indirect. In the indirect case, electrons/positrons emit bremsstrahlung photons by interaction with the surrounding material that hit at least one crystal. Photons can also come from annihilating positrons, with specific energy of 511 keV. For HED, because of the shielding, about 98 % of the energy deposition is due to indirect hits into the BGO crystals. For LED, direct hits are more important: about 72 % of the energy deposition. This explains why the effective area of LED is larger than HED when considering incident electrons/positrons. The effective area is calculated as the geometrical area (≈ 900 cm^2 for HED and ≈ 1024 cm^2 for LED) multiplied by the probability of an incident TEB electron to deposit more than 300 keV into at least one BGO crystal (for HED), or more than 50 keV into at least one CZT pixel (for LED).

At the end of the second stage, a simulation data set in the form of a list of detected time and energy counts is generated. To be able to completely neglect the simulation noise, it is required to have at least 1,000,000 counts on each detector to build each energy spectrum and calculate the effective areas. The final modeled spectra also include a background component build from real background data.

A key feature of performing spectral analysis on the TEB, instead of TGF, is that the energy spectrum of the constituting electrons and positrons above 100 km altitude is only weakly dependent on the following parameters:

- the radial distance between the TEB center and the ISS. The concept of radial is presented more precisely in the supporting information, Figure A.1.
- the beaming and the tilt angles of the source TGF.
- the source altitude of the TGF, if set between 10 and 15 km.

Actually, we found that the spectrum of the source TGF mostly affects the spectrum of the detected TEB. This permit a substantial simplification of the problem as it reduces drastically the number of free parameters to include in the analysis. Since these three points are crucial for this analysis, we provide in the supporting information document more detailed arguments and simulation results supporting those three points. It includes the results of the procedure described below if applied to source TGF altitudes of 10 and 15 km, and various opening angle distribution and tilt angles. The effect of the source TGF altitude is small and does not affect significantly the results presented next (this issue discussed into details in the supporting information, section B). In the following, we fix the model to the "consensus" source altitude to 12 km, the angular distribution to $\sigma = 20^o$, and the tilt angle to 0^o.

The simulated spectra are evaluated with respect to the observation, separately for the LED (50 to 370 keV) and the HED (0.3 to 40 MeV), and with both detectors together. To compare the modeling results to the observation, we use a likelihood analysis, a χ^2 analysis (Eadie et al., 1971; Martin, 1971; Lyons, 1986), and the effective LED/HED area ratio. Note that these three methods are not independent as they used on the same datasets: the list of measured and simulated energy by HED and LED, taken together or separately.

For the likelihood analysis, a value of $-2\,ln(\mathcal{L})$, the Negative Log-Likelihood, is calculated. The model with the lowest value of $-2\,ln(\mathcal{L})$ is considered being the best description of the observation. Models are considered to be also possible if their $-2\,ln(\mathcal{L})$ values have a difference that is less than a threshold value τ. We calculated that $\tau \approx 5$ for a confidence level of about 99%, similar to the one used by Mailyan et al. (2016)

for Fermi-GBM observations. This value assumes that $-2\,ln(\mathcal{L})$ evolves following approximately a normal (a.k.a. Gaussian) distribution with respect to the free parameter(s). In the following, we present the values Δ_{mle}, that are the values of $-2\,ln(\mathcal{L})$ subtracted by the value of $-2\,ln(\mathcal{L})$ for the best model. Therefore the best model has $\Delta_{mle} = 0$ and compatible models have $\Delta_{mle} \leq \tau$. A verification if a given model was found not better than another just because of random fluctuations ("by chance") is also performed.

For completeness, we also provide a reduced χ^2 value, noted χ^2_r. If χ^2_r is below a critical value, the model is considered compatible with the measurement, and above the model is considered incompatible. The Pearson's χ^2 method is affected by choice of binning (i.e. energy intervals chosen to built the spectra). To mitigate this effect, we chose a binning with at least 7 measurement counts on each bin for HED, and at least 10 for LED. These two binnings are used to make the spectra presented in Figure 2.b. Given the used binning, the critical value $\chi^2_{r,c}$ is 1.94 (8 degrees of freedom) for LED, 1.75 for HED (12 degrees of freedom) and 1.57 for the combination of both (20 degrees of freedom).

Compared to the Pearson's χ^2, the maximum likelihood analysis presents the advantage of not relying on a bining of the measurement data: it keeps all its granularity, i.e. no information is lost by binning the measurements. The maximum likelihood analysis is better suited than the χ^2 to estimate which model is the best description of the observation (see, for example, Hauschild and Jentschel (2001))

5 Results and discussion

Table 1 summarizes the results of this study. The models are sorted according the prevalence of high energies (also called "hardness") or, equivalently, by decreasing LED/HED effective area ratio. As indicated in the previous section, three main evaluation criteria are presented: the reduced Pearson's χ^2_r, the maximum likelihood, and the LED/HED effective area ratio.

Concerning the LED spectral fits (table 1), all the models give good fits, using the χ^2_r or the Maximum likelihood analysis. We interpret this as the energy range of 50 keV to 370 keV being too narrow to discriminate between the models. Concerning the HED spectral fits, looking at the χ^2_r values, only the 160 MV leader model is found incompatible. This criterion gives similar conclusions when LED and HED spectra are combined.

The maximum likelihood analysis on the HED spectrum indicates that the best model is for $\epsilon = 8$ MeV. The fit for $\epsilon = 7.3$ MeV is also very close. It indicates that the leader 300 MV model and harder spectra are also possible explanations. If LED and HED spectra are combined, the best model is then $\epsilon = 10$ MeV (but $\epsilon = 8$ MeV is a very close fit here as well), and only models with $\epsilon = 6.5$ MeV or greater are compatible.

Since 307 counts are observed for LED (> 50 keV) and 168 for HED (> 300 keV), the observed ratio is 1.83. Considering that the two count numbers individually follow a Poisson statistic (but the ratio does not), the uncertainty on the ratio is ± 0.35 (95% interval). It implies that, using this criterion, the two leader-based source TGF spectral models (160 MV and 300 MV) are incompatible. The effective area ratio analysis indicates that the models with $\epsilon \geq 6.5$ MeV are compatible. In particular we cannot exclude $\epsilon = 8$ and $\epsilon = 10$ MeV. A similar conclusion is obtained with the maximum likelihood analysis (see last paragraph).

For this event, TGF spectra harder than previously expected are possible. AGILE did report observations of TGF surprisingly hard (up to 100 MeV), but they were later found explainable from instrumental effects (Marisaldi et al., 2019). It does not exclude that the mechanism presented in (Celestin et al., 2012), used first to explain TGF spectra up to 100 MeV, could not be responsible for producing TGFs with a bit harder energy spectra than fully-developed RREA.

The results presented in this article are also only valid for a single event, and it does not imply that leader models with potentials of 300 MV or less could explain other TGF (and TEB) events. It is also possible that because our method relies on the detection of a TEB, we are biased towards a population of strong TGFs, necessitating fully-developed RREAs. TGFs that could originate from non-fully-developed RREAs (leader models) may never (or very rarely) produce a detectable TEB. This question could be addressable in the future, by applying this analysis to more TEB events. We list possibilities of new studies in the next section.

Finally, table 1 also indicates the positron/electron ratio. The model giving the best fit ($\epsilon = 10$ MeV) gives a ratio of 18.3%, and the range of compatible models give a ratio ranging from 15.2% to 18.3%. This range is compatible with estimations from the Fermi space telescope team (Briggs et al., 2011).

6 Conclusions and future work

We reported the observation of a Terrestrial Electron Beam by ASIM on March 24, 2019, originating from the rainbands of the tropical cyclone Johanina. The associated lightning stroke was detected by the GLD360 network (VAISALA) in close temporal association and very close to the ISS's south magnetic field line footpoint. The TEB spectrum was resolved down to 50 keV for the first time, using ASIM's low energy detector. A method to constrain the TGF source energy spectrum based on the TEB detection was presented. It relies on a key reduction of the number of free parameters (altitude, angular distribution, radial distance) possible due to TEB's properties. Comprehensive Monte-Carlo simulations were performed to reproduce the observation, assuming several (energy) spectral shapes of the source TGF. Using three criteria to evaluate the simulation results with respect to the observation (Maximum likelihood, Pearson's χ_r^2 and LED/HED count ratio), we showed that source TGF with, at least, a fully-developed RREA spectrum $\propto E^{-1}\exp(-E/\epsilon)$ (with $\epsilon \geq 6.5$ MeV, $E_m = 40$ MeV) is compatible with the observation. We could not exclude harder models with $\epsilon = 8$ MeV ($E_m = 40$ MeV) and 10 MeV ($E_m = 40$ MeV), that could potentially be explained by non-equilibrium acceleration of energetic electrons in lightning (Celestin et al., 2012).

In the future, we expect that a larger number of events will be processed using the method presented in this article. For ASIM, it will not be possible before several more years of data gathering, since it currently detects about 4 TEB a year, and not all of them present LED data (only turned ON during the night time of the ISS) or enough counts on LED and HED. In principle, the method presented in this article could also be applied/translated to events from the Fermi GBM TGF/TEB catalog (Roberts et al., 2018), that currently contains about 30 TEB events. Fermi GBM has and high energy (BGO-based) detectors that covers an energy range of $\approx$ 150 keV to $\approx$ 30 MeV. GBM's NaI detectors could also be used in principle (with an energy range of a few keV to 1 MeV) but no TEB spectrum using it was reported yet. Since TEB events present lower fluxes (counts per second) than TGFs (typically 20 times), it makes the spectral analysis much less challenging than for TGF events. Instrumental effects (dead-time, pile-up), affecting TGF analysis, can be mostly (if not totally) ignored for TEB spectral analysis.

Model	Effective area in cm^2		Effective area ratio	Maximum likelihood analysis result Δ_{mle}			Pearson's χ^2_r			e^+/e^- ratio
	LED	HED		LED	HED	Co.	LED	HED	Co.	
"Leader 160 MV" $\varepsilon = 4.3$ MeV $E_m = 19.2$ MeV	122.0	43.7	2.79	**0**	19.0	22.5	**0.84**	1.97	1.66	10.3 %
"Leader 300 MV" $\varepsilon = 4.7$ MeV $E_m = 32$ MeV	141.5	61.0	2.32	**0**	**3.4**	7.1	**0.88**	**1.04**	**1.31**	13.3 %
$\varepsilon = 6.5$ MeV $E_m = 40$ MeV	156.0	74.4	**2.10**	**0.2**	**0.8**	**3.1**	**0.89**	**0.87**	**1.27**	15.2 %
$\varepsilon = 7.3$ MeV $E_m = 40$ MeV	162.2	80.4	**2.02**	**0.3**	**0.2**	**1.9**	**0.88**	**0.85**	**1.28**	16.1 %
$\varepsilon = 8$ MeV $E_m = 40$ MeV	168.4	85.5	**1.97**	**0.5**	**0**	**1.1**	**0.89**	**0.84**	**1.29**	16.8 %
$\varepsilon = 10$ MeV $E_m = 40$ MeV	177.8	94.7	**1.88**	**0.5**	**1.0**	**0**	**0.90**	**0.83**	**1.30**	18.3 %
Compatibility range	n.a.		1.82±0.35	≤ 5			≤ 1.94	≤ 1.75	≤ 1.57	n.a.

Table 1. Table summarizing the comparison of the tested spectral models with the measurement. Three main criteria are presented: the LED/HED effective area ratio, the maximum likelihood and the Pearson's χ^2_r. "Co." stands for the LED and HED combination. The compatibility range for the different criteria are also indicated. Bold values indicate compatible models for the given criteria (column).

Figure 1. Image from geostationary satellite Meteosat-11 around 00:30 UTC, about 1 minute and 53 seconds before the ASIM trigger. The image comes from the optical band 4 (3.9 μm, 3 km resolution). The tropical cyclone Joaninha can be seen in the south-east part of the picture and extends over a thousand of kilometers. The positions of the International Space Station (ISS), the GLD360 match (V), and the magnetic field line footpoint (M) are indicated. The track of the Earth's magnetic field line (blue dashed line) and of ISS trajectory (green dashed line) are also showed. Point V is very close to M in both location ($\Delta r = 4.82$ km) and time ($\Delta t = 1.44$ ms), and is located in the north-western rainbands of the cyclone.

7 Acknowledgments

The data presented in this article is available in the following Zenodo repository: `https://doi.org/10.5281/zenodo.4264459`

This work was supported by the European Research Council under the European Union's Seventh Framework Program (FP7/2007-2013)/ERC grant agreement n. 320839 and the Research Council of Norway under contract 223252/F50 (CoE). ASIM is a mission of ESA's SciSpace Programme for scientific utilization of the ISS and non-ISS space exploration platforms and space environment analogues. This study has received funding from the European Union's Horizon 2020 research and innovation programme under the Marie Sklodowska-Curie grant agreement SAINT 722337. ASIM was funded through the ESA ELIPS program, through contracts with TERMA and Danish Technical University (DTU) in Denmark, University of Bergen (UB) in Norway and University of Valencia (UV) in Spain. Additional funding was supported by the ESA PRODEX contracts PEA 4000105639 and 4000111397 to DTU and ESA PRODEX contract 4000102100 and by Norwegian Research Council to UB. The ASIM Science Data Centre (ASDC) at DTU is supported by PRODEX contract PEA 4000115884 and by PRODEX contract PEA4000123438 at UB. The ASIM Science Data Centre and data analysis activities at the UV are supported by the MINECO Research Grants ESP2015- 69909-C5-1-R and ESP2017-86263-C4-1-R.

We thank Vaisala Inc. for access to the GLD360 data. For more information, see `https://www.GLD360.com/en/products/systems/lightning129detection-networks`.

We acknowledge EUMETSAT for making accessible images from the Meteosat-11 geostationary satellite and the MCFETCH service (`https://mcfetch.ssec.wisc.edu/`) from the Satellite Data Services (SDS) group, at the University of Wisconsin-Madison Space Science and Engineering Center (SSEC), that is responsible for the access, maintenance, and distribution of real-time and archive weather satellite data.

The simulations were performed on resources provided by UNINETT Sigma2 - the National Infrastructure for High Performance Computing and Data Storage in Norway, under project no. NN9526K.

The Geant4-based model for Terrestrial Gamma-ray Flash (TGF) and associated electrons and positrons propagation in Earth atmosphere and environment (magnetic

field) is available in the following GitHub repository: `https://github.com/DavidSarria89/TGF-Propagation-Geant4`, or the DOI: `https://doi.org/10.5281/zenodo.2597039`.

References

Babich, L. P., Donskoy, E. N., Kutsyk, I. M., & Roussel-Dupré, R. A. (2005). The feedback mechanism of runaway air breakdown. *Geophysical Research Letters*, *32*(9). doi: 10.1029/2004GL021744

Bowers, G. S., Smith, D. M., Martinez-McKinney, G. F., Kamogawa, M., Cummer, S. A., Dwyer, J. R., ... Kawasaki, Z. (2017). Gamma Ray Signatures of Neutrons From a Terrestrial Gamma Ray Flash. *Geophysical Research Letters*, *44*(19). doi: 10.1002/2017GL075071

Briggs, M. S., Connaughton, V., Wilson-Hodge, C., Preece, R. D., Fishman, G. J., Kippen, R. M., ... Smith, D. M. (2011). Electron-positron beams from terrestrial lightning observed with Fermi GBM. *Geophysical Research Letters*, *38*, L02808. doi: 10.1029/2010GL046259

Briggs, M. S., Fishman, G. J., Connaughton, V., Bhat, P. N., Paciesas, W. S., Preece, R. D., ... Chekhtman, A. (2010). First results on terrestrial gamma ray flashes from the Fermi Gamma-ray Burst Monitor. *Journal of Geophysical Research (Space Physics)*, *115*, A07323. doi: 10.1029/2009JA015242

Celestin, S., & Pasko, V. P. (2011). Energy and fluxes of thermal runaway electrons produced by exponential growth of streamers during the stepping of lightning leaders and in transient luminous events. *Journal of Geophysical Research (Space Physics)*, *116*, A03315. doi: 10.1029/2010JA016260

Celestin, S., Xu, W., & Pasko, V. P. (2012). Terrestrial gamma ray flashes with energies up to 100 MeV produced by nonequilibrium acceleration of electrons in lightning. *Journal of Geophysical Research (Space Physics)*, *117*(A5). doi: 10.1029/2012JA017535

Celestin, S., Xu, W., & Pasko, V. P. (2015). Variability in fluence and spectrum of high-energy photon bursts produced by lightning leaders. *Journal of Geophysical Research (Space Physics)*, *120*(12), 10,712–10,723. doi: 10.1002/2015JA021410

Chanrion, O., Bonaventura, Z., Çinar, D., Bourdon, A., & Neubert, T. (2014). Runaway electrons from a 'beam-bulk' model of streamer: application to TGFs.

Environmental Research Letters, *9*(5), 055003. doi: 10.1088/1748-9326/9/5/055003

Chanrion, O., Neubert, T., Lundgaard Rasmussen, I., Stoltze, C., Tcherniak, D., Jessen, N. C., … Lorenzen, M. (2019). The Modular Multispectral Imaging Array (MMIA) of the ASIM Payload on the International Space Station. *ßr*, *215*, 28. doi: 10.1007/s11214-019-0593-y

Cohen, M. B., Inan, U. S., Said, R. K., Briggs, M. S., Fishman, G. J., Connaughton, V., & Cummer, S. A. (2010). A lightning discharge producing a beam of relativistic electrons into space. *Geophysical Research Letters*, *37*(18), L18806. doi: 10.1029/2010GL044481

Dwyer, J. R. (2008). Source mechanisms of terrestrial gamma-ray flashes. *Journal of Geophysical Research (Atmospheres)*, *113*(D10), D10103. doi: 10.1029/2007JD009248

Dwyer, J. R. (2012). The relativistic feedback discharge model of terrestrial gamma ray flashes. *Journal of Geophysical Research (Space Physics)*, *117*(A2), A02308. doi: 10.1029/2011JA017160

Dwyer, J. R., Grefenstette, B. W., & Smith, D. M. (2008). High-energy electron beams launched into space by thunderstorms. *Geophysical Research Letters*, *35*, L02815. doi: 10.1029/2007GL032430

Dwyer, J. R., Rassoul, H. K., Al-Dayeh, M., Caraway, L., Chrest, A., Wright, B., … others (2005). X-ray bursts associated with leader steps in cloud-to-ground lightning. *Geophysical Research Letters*, *32*(1).

Dwyer, J. R., Rassoul, H. K., Al-Dayeh, M., Caraway, L., Wright, B., Chrest, A., … others (2004). Measurements of X-ray emission from rocket-triggered lightning. *Geophysical research letters*, *31*(5).

Dwyer, J. R., Schaal, M., Rassoul, H. K., Uman, M. A., Jordan, D. M., & Hill, D. (2011). High-speed X-ray images of triggered lightning dart leaders. *Journal of Geophysical Research:Atmospheres*, *116*(D15), D20208. doi: 10.1029/2011JD015973

Dwyer, J. R., Smith, D. M., Cummer, S. A., ., ., ., … . (2012). High-Energy Atmospheric Physics: Terrestrial Gamma-Ray Flashes and Related Phenomena. *Space Science Reviews*, *173*(1-4), 133–196. doi: 10.1007/s11214-012-9894-0

Dwyer, J. R., Uman, M. A., Rassoul, H. K., Al-Dayeh, M., Caraway, L., Jerauld, J.,

… Wright, B. (2003). Energetic Radiation Produced During Rocket-Triggered Lightning. *Science*, *299*, 694–697. doi: 10.1126/science.1078940

Eadie, W. T., Drijard, D., James, F. E., Roos, M., & Sadoulet, B. (1971). *Statistical methods in experimental physics.* Amsterdam: North-Holland. Retrieved from `https://cds.cern.ch/record/100342`

Fishman, G. J., Bhat, P. N., Mallozzi, R., Horack, J. M., Koshut, T., Kouveliotou, C., … Christian, H. J. (1994). Discovery of Intense Gamma-Ray Flashes of Atmospheric Origin. *Science*, *264*(5163), 1313–1316. doi: 10.1126/science.264.5163.1313

Gjesteland, T. (2012). *Properties of Terrestrial Gamma ray Flashes. Modelling and Analysis of BATSE and RHESSI data* (PhD Thesis, The University of Bergen). Retrieved from `http://bora.uib.no/handle/1956/6203`

Gurevich, A. V. (1961). On the theory of runaway electrons. *Sov. Phys. JETP*, *12*(5), 904–912.

Gurevich, A. V., Milikh, G. M., & Roussel-Dupre, R. (1992). Runaway electron mechanism of air breakdown and preconditioning during a thunderstorm. *Physics Letters A*, *165*(5-6), 463–468.

Hauschild, T., & Jentschel, M. (2001). Comparison of maximum likelihood estimation and chi-square statistics applied to counting experiments. *Nuclear Instruments and Methods in Physics Research Section A: Accelerators, Spectrometers, Detectors and Associated Equipment*, *457*(1), 384 – 401. Retrieved from `http://www.sciencedirect.com/science/article/pii/S0168900200007567` doi: 10.1016/S0168-9002(00)00756-7

Kohn, C., & Ebert, U. (2015). Calculation of beams of positrons, neutrons, and protons associated with terrestrial gamma ray flashes. *Journal of Geophysical Research:Atmospheres*, *120*(4), 1620–1635. doi: 10.1002/2014JD022229

Lindanger, A., Marisaldi, M., Maiorana, C., Sarria, D., Albrechtsen, K., Østgaard, N., … Verrecchia, F. (2020). The 3rd AGILE Terrestrial Gamma Ray Flash Catalog. Part I: Association to Lightning Sferics. *Journal of Geophysical Research:Atmospheres*, *125*(11), e2019JD031985. doi: 10.1029/2019JD031985

Lyons, L. (1986). *STATISTICS FOR NUCLEAR AND PARTICLE PHYSICISTS.*

Mailyan, B. G., Briggs, M. S., Cramer, E. S., Fitzpatrick, G., Roberts, O. J., Stanbro, M., … Dwyer, J. R. (2016). The spectroscopy of individual terrestrial gamma-ray flashes: Constraining the source properties. *Journal of Geophysical Research (Space Physics)*, *121*(A10), 11. doi: 10.1002/2016JA022702

Mailyan, B. G., Xu, W., Celestin, S., Briggs, M. S., Dwyer, J. R., Cramer, E. S., … Stanbro, M. (2019). Analysis of Individual Terrestrial Gamma-Ray Flashes With Lightning Leader Models and Fermi Gamma-Ray Burst Monitor Data. *Journal of Geophysical Research (Space Physics)*, *124*(8), 7170–7183. Retrieved from `https://agupubs.onlinelibrary.wiley.com/doi/abs/10.1029/2019JA026912` doi: 10.1029/2019JA026912

Marisaldi, M., Fuschino, F., Tavani, M., Dietrich, S., Price, C., Galli, M., … Vercellone, S. (2014). Properties of terrestrial gamma ray flashes detected by AGILE MCAL below 30 MeV. *Journal of Geophysical Research (Space Physics)*, *119*, 1337–1355. doi: 10.1002/2013JA019301

Marisaldi, M., Galli, M., Labanti, C., Østgaard, N., Sarria, D., Cummer, S. A., … Verrecchia, F. (2019). On the High-Energy Spectral Component and Fine Time Structure of Terrestrial Gamma Ray Flashes. *Journal of Geophysical Research:Atmospheres*, *124*(14), 7484–7497. Retrieved 2021-01-22, from `https://onlinelibrary.wiley.com/doi/abs/10.1029/2019JD030554` doi: 10.1029/2019JD030554

Martin, B. R. (1971). *Statistics for physicists [by] B. R. Martin.* Academic Press London, New York.

Moss, G. D., Pasko, V. P., Liu, N., & Veronis, G. (2006). Monte Carlo model for analysis of thermal runaway electrons in streamer tips in transient luminous events and streamer zones of lightning leaders. *Journal of Geophysical Research (Space Physics)*, *111*, 2307. doi: 10.1029/2005JA011350

Neubert, T., Østgaard, N., Reglero, V., Blanc, E., Chanrion, O., Oxborrow, C. A., … Bhanderi, D. D. V. (2019). The ASIM Mission on the International Space Station. *Space Science Reviews*, *215*(2), 26. Retrieved 2021-01-22, from `http://link.springer.com/10.1007/s11214-019-0592-z` doi: 10.1007/s11214-019-0592-z

Neubert, T., Østgaard, N., Reglero, V., Chanrion, O., Heumesser, M., Dimitriadou, K., … Eyles, C. J. (2019). A terrestrial gamma-ray flash and ionospheric ultraviolet emissions powered by lightning. *Science*, eaax3872. Retrieved 2021-01-20, from `https://www.sciencemag.org/lookup/doi/10.1126/`

`science.aax3872` doi: 10.1126/science.aax3872

Østgaard, N., Balling, J. E., Bjørnsen, T., Brauer, P., Budtz-Jørgensen, C., Bujwan, W., ... Yang, S. (2019). The Modular X- and Gamma-Ray Sensor (MXGS) of the ASIM Payload on the International Space Station. *Space Science Reviews*, *215*, 23. doi: 10.1007/s11214-018-0573-7

Østgaard, N., Neubert, T., Reglero, V., Ullaland, K., Yang, S., Genov, G., ... Al-nussirat, S. (2019). First 10 Months of TGF Observations by ASIM. *Journal of Geophysical Research:Atmospheres*, *124*(24), 14024–14036. Retrieved 2021-01-20, from `https://onlinelibrary.wiley.com/doi/10.1029/2019JD031214` doi: 10.1029/2019JD031214

Roberts, O. J., Fitzpatrick, G., Stanbro, M., McBreen, S., Briggs, M. S., Holzworth, R. H., ... Mailyan, B. G. (2018). The First Fermi-GBM Terrestrial Gamma Ray Flash Catalog. *Journal of Geophysical Research (Space Physics)*, *123*, 4381–4401. doi: 10.1029/2017JA024837

Rudlosky, S. D., Peterson, M. J., & Kahn, D. T. (2017). GLD360 Performance Relative to TRMM LIS. *Journal of Atmospheric and Oceanic Technology*, *34*(6), 1307 – 1322. doi: 10.1175/JTECH-D-16-0243.1

Sarria, D., Blelly, P.-L., & Forme, F. (2015). MC-PEPTITA: A Monte Carlo model for Photon, Electron and Positron Tracking In Terrestrial Atmosphere—Application for a terrestrial gamma ray flash. *Journal of Geophysical Research (Space Physics)*, *120*(5), 3970–3986. Retrieved from `https://agupubs.onlinelibrary.wiley.com/doi/abs/10.1002/2014JA020695` doi: 10.1002/2014JA020695

Sarria, D., Kochkin, P. O., Østgaard, N., Lehtinen, N. G., Mezentsev, A., Marisaldi, M., ... Eyles, C. (2019). The First Terrestrial Electron Beam Observed by the Atmosphere-Space Interactions Monitor. *Journal of Geophysical Research (Space Physics)*, *124*(12), 10,497–10,511. doi: 10.1029/2019JA027071

Sarria, D., Rutjes, C., Diniz, G., Luque, A., Ihaddadene, K. M. A., Dwyer, J. R., ... Ebert, U. (2018). Evaluation of Monte Carlo tools for high-energy atmospheric physics II: relativistic runaway electron avalanches. *Geoscientific Model Development*, *11*, 4515–4535. doi: 10.5194/gmd-11-4515-2018

Skeltved, A. B., Østgaard, N., Carlson, B. E., Gjesteland, T., & Celestin, S. (2014). Modeling the relativistic runaway electron avalanche and the feedback mechanism with GEANT4. *Journal of Geophysical Research (Space Physics)*, *119*, 9174–9191. doi: 10.1002/2014JA020504

Skeltved, A. B., Østgaard, N., Mezentsev, A., Lehtinen, N. G., & Carlson, B. E. (2017). Constraints to do realistic modeling of the electric field ahead of the tip of a lightning leader. *Journal of Geophysical Research:Atmospheres*, *122*(15), 8120–8134. Retrieved from https://agupubs.onlinelibrary.wiley.com/doi/abs/10.1002/2016JD026206 doi: 10.1002/2016JD026206

Smith, D. M., Grefenstette, B. W., Splitt, M., Lazarus, S. M., Rassoul, H. K., Coleman, L. M., ... Takahashi, Y. (2006). The Anomalous Terrestrial Gamma-ray Flash of 17 January 2004. *AGU Fall Meeting Abstracts*, AE31A–1040.

Smith, D. M., Lopez, L. I., Lin, R. P., & Barrington-Leigh, C. P. (2005). Terrestrial Gamma-Ray Flashes Observed up to 20 MeV. *Science*, *307*, 1085–1088. doi: 10.1126/science.1107466

Stanbro, M., Briggs, M. S., Roberts, O. J., Cramer, E., Dwyer, J. R., Holzworth, R., ... Xiong, S. L. (2019). A Fermi Gamma-Ray Burst Monitor Event Observed as a Terrestrial Gamma-Ray Flash and Terrestrial Electron Beam. *Journal of Geophysical Research (Space Physics)*, *124*(12), 10580–10591. Retrieved from https://agupubs.onlinelibrary.wiley.com/doi/abs/10.1029/2019JA026749 doi: 10.1029/2019JA026749

Ursi, A., Guidorzi, C., Marisaldi, M., Sarria, D., & Frontera, F. (2017). Terrestrial gamma-ray flashes in the BeppoSAX data archive. *Journal of Atmospheric and Solar-Terrestrial Physics*, *156*, 50–56. doi: 10.1016/j.jastp.2017.02.014

Wilson, C. T. R. (1924). The electric field of a thundercloud and some of its effects. *Proceedings of the Physical Society of London*, *37*, 32D–37D.

Xu, W., Celestin, S., Pasko, V. P., & Marshall, R. A. (2019). Compton Scattering Effects on the Spectral and Temporal Properties of Terrestrial Gamma-Ray Flashes. *Journal of Geophysical Research (Space Physics)*, *124*(8), 7220–7230. Retrieved from https://agupubs.onlinelibrary.wiley.com/doi/abs/10.1029/2019JA026941 doi: 10.1029/2019JA026941

Supporting Information

Article: *Constraining spectral models of a terrestrial gamma-ray flash from a terrestrial electron beam observation by the Atmosphere-Space Interactions Monitor*

Authors: *D. Sarria*[1], *N. Østgaard*[1], *P. Kochkin*[1], *N. Lehtinen*[1], *A. Mezentsev*[1], *M. Marisaldi*[1], *A. Lindanger*[1], *C. Maiorana*[1], *B. E. Carlson*[1,2], *T. Neubert*[3], *V. Reglero*[4], *K. Ullaland*[1], *S.Yang*[1], *G. Genov*[1], *B. H. Qureshi*[1], *C. Budtz-Jørgensen*[3], *I. Kuvvetli*[3], *F. Christiansen*[3], *O. Chanrion*[3], *J. Navarro-González*[4], *P. Connel*[4], *C. Eyles*[4]

1 : Birkeland Centre for Space Science, University of Bergen, Bergen, Norway

2 : Carthage College, Kenosha, Wisconsin, United States

3 : National Space Institute, Technical University of Denmark, Lyngby, Denmark

4 : University of Valencia, Valencia, Spain

This document aims to provide support to the main text about the weak dependence of the detected TEB spectrum on (1) the radial distance between the TEB center and the ISS, (2) the altitude of the source TGF (if set between 10 and 15 km), (3) the opening and the tilt angles of the source TGF. In section A, we present simulation results of the TEB energy spectra for the different set of parameters (radial distance, altitude, opening and tilt angles). Since the dependence on the TGF source altitude is the most noticeable (even if weak), we present in Section B the resulting tables of the full spectral analysis, but for TGF source altitudes of 10 and 15 km (the case of 12 km is considered in the main article). It demonstrate that the effect of the altitude is indeed weak . In section C, we present the binned energy spectra for LED and HED (and the combination) used to calculate the χ_r^2 values in the main text.

A Parameter reduction for the energy spectrum analysis

In this section, we provide detailed justifications on why when performing spectral analysis on the Terrestrial Electron Beam (TEB), the shape of the recorded energy spectrum above 100 km altitude is only weakly dependent on the following parameters:

- the radial distance between the TEB center and the ISS, see section A.1
- the altitude, if set between 10 and 15 km, see section A.2
- the opening and the tilt angles, see section A.3

This permits an essential parameter reduction to be able to perform a more constrained spectral analysis for the source TGF spectrum (producing the TEB), see the main text. However, these four parameters can have dramatic effect on the fluence (particles per cm^2) of the TEB, but this is not considered here because it only corresponds to a scale factor and has no effect on the spectral shape and the spectral analysis. Note also that this scale factor corresponds to the brightness of the source TGF and is a free parameter.

This key feature permits a big simplification of the problem as it reduces drastically the number of free parameters to include in the analysis. However, compared to TGF-only simulations, TGF+TEB simulations also present some disadvantages:

- they require more computation time, as accounting for electron/positron propagating in a large scale (Earth) magnetic field is much more computationally expensive than simulating only photon propagation.
- no detector response matrix can be used (this is only possible for incident photons) hence simulations using the full mass model must be performed for each source TGF spectrum, that is also computationally much more expensive.

In the following we present several simulated TEB energy spectra at satellite altitude (about 400 km for the ISS). They would be similar if detected anywhere between 100 km altitude and the satellite's altitude, because the remaining atmosphere above ≈100 km is very thin and cannot affect significantly the energetic electrons/positrons ($>$ 400 keV). The presented spectra are also shown with a minimal energy of 400 keV, because electrons with lower energies are not expected to be detected by ASIM. Positrons with energies $<$ 400 keV will produce pairs of 511 keV photons after annihilating after losing all their kinetic energy in the material surrounding the detectors. For all the simulations presented in this supporting information, the source TGF is assumed to have a standard fully-developed RREA spectrum $\propto 1/E \exp\left(-E/\epsilon\right)$, $\epsilon = 7.3$ MeV. Throughout the document, the energy spectrum curves are normalized to be equal to 1 at 1 MeV. Note that the choice of normalization does not really matter as it can be arbitrary, depending on the source brightness, that has a large range possible values ($\sim 10^{16}$ to $\sim 10^{20}$).

A.1 Effect of the radial distance between detector and TEB's center

For clarity, Figure A.1 presents a sketch to define the concept of radial distance. Figure A.2 shows simulations results of TEB electron energy spectra (at satellite altitude) inside several radial distance rings between the center of the TEB and the detector. The spectrum of a TEB only weakly varies with the radial distance between the TEB center and the detector. This is because electrons/positrons produced at a similar altitude, 80 km apart, have similar energy distribution. In addition the gyration motion of electrons/positrons along field lines also shuffles their positions. Above a radial distance of 80 km, we may observe a more significant difference (though we did not reach enough statistics in our simulations to check this precisely). In addition, 80 km from the center, the fluence (particles/cm^2) is about 25 times lower than in the center (point 0) and decreases even more with increasing radial distance, hence it is much less likely that the TEB could be detected from there.

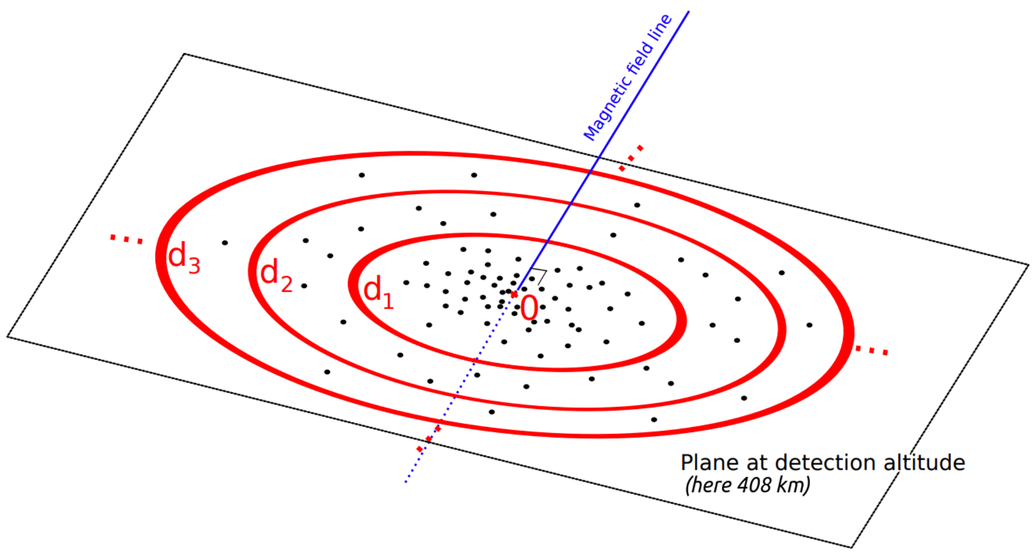

Figure A.1: Illustration of the concept of radial distance. The 0 is the center of the electron beam. The radial distance in the distance between this 0 and another point in the plane. The black dots represent the positions of electrons or positrons (there are millions of particles in the actual simulation data). The red rings are radial distance intervals at which electrons are collected. The spectra presented in Figure A.2 are built at given radial distance intervals.

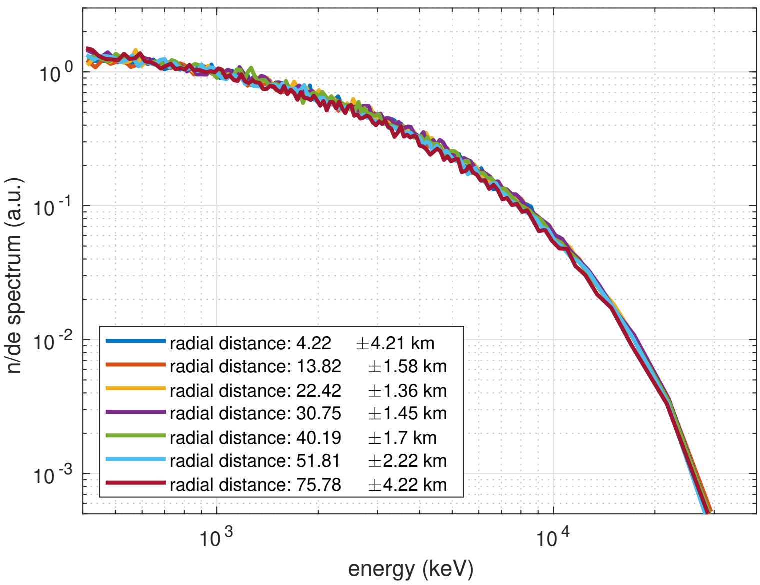

Figure A.2: TEB electron energy spectrum inside several radial distance rings between the center of the electron beam and the detector. The radial distance bins (i.e. intervals) and the energy bins are chosen to contain a similar number of particles. We observe very minor differences for any of the tested radial distances.

A.2 Effect of the altitude of the source TGF

The high energy part of the TGF spectrum (> 4 MeV) is affecting the production of energetic electrons and positrons (able to escape the atmosphere). This part of the spectrum remains similar after propagation to ≈ 100 km (and therefore higher altitudes since the effect of the atmosphere becomes negligible above) if the TGF source is placed from 10 km to 15 km altitude (in the main text, an altitude of 12 km is set). However, we may observe a more important variability for a broader altitude range but it is not relevant for TGFs. To justify qualitatively the previous statements, we performed extensive Monte-Carlo simulations. Figure A.3 presents the results, together with a quantification of the differences (lower panel). The resulting TEB spectra show a relative difference of less than 20% (absolute value) for most of the energy range, with an average of about 12% (absolute value). With only this information, we concede that it is not obvious that the source altitude will have only a weak effect on the results of the spectral analysis. This is why we also proceeded to the full spectral analysis for source TGF altitudes of 10 and 15 km, and built tables like Table 1 but for these source TGF altitudes. They are shown as Tables B.1 and B.2 (Table in the main text 1 is for 12 km). By looking at these tables, we can confirm that the TGF source altitude has only a weak effect on the results of the spectral analysis.

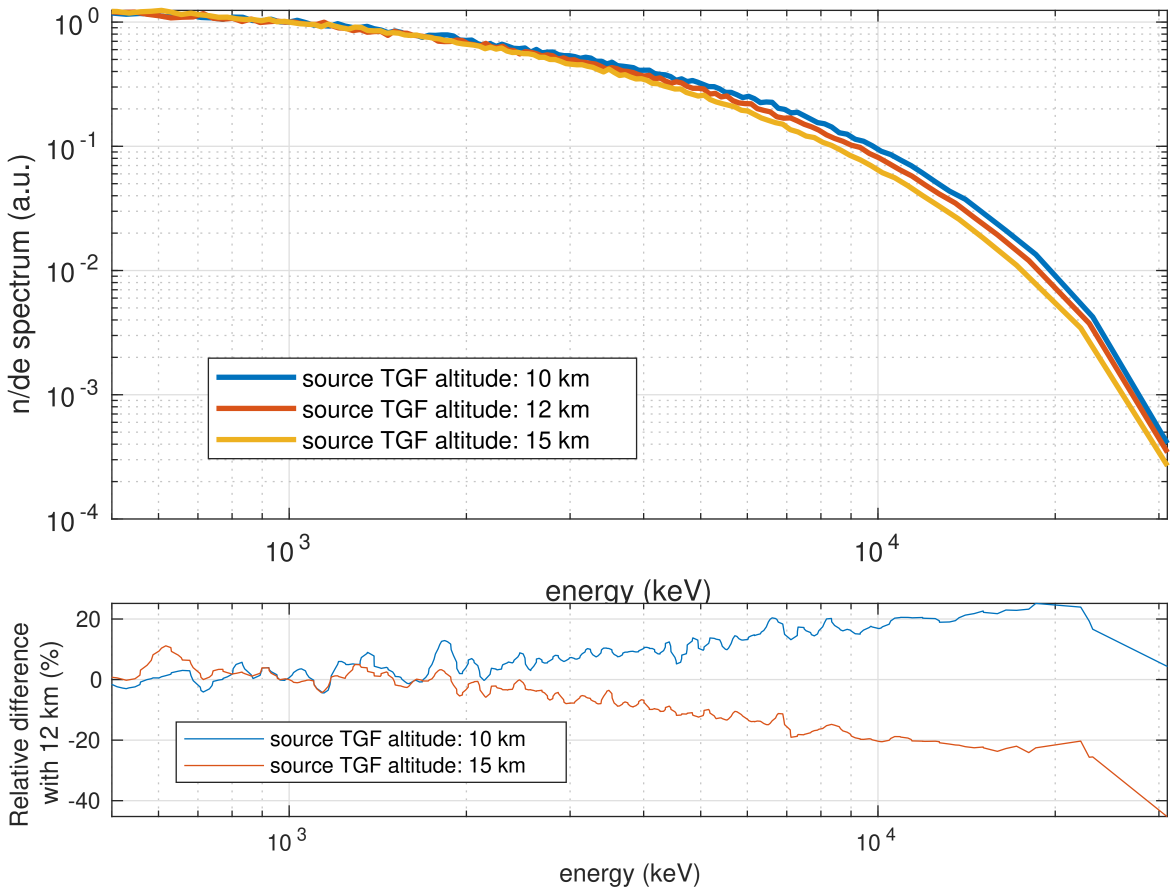

Figure A.3: Simulation results. The energy bins are chosen to contain a similar number of particles. TEB energy spectrum at satellite altitude, assuming different source TGF altitudes. Relatively small differences are observed.

A.3 Effect of the beaming and tilt angles of the source TGF

TGFs photons are forming a beam that is parameterized by an angle σ_θ (the source TGF is assumed to be beamed as a cone to make the discussion easier) and a tilt angle ρ with respect to the local vertical. We define the tilt angle ρ as follow: consider a plane defined by the TGF beam (center) direction, the local magnetic field direction and the TGF source (point) location. The tilt angle ρ as the angle the center of TGF beam is making with the local vertical (upwards), in the previous plane.

For this event, the angle between the direction of the local magnetic field and the local vertical is 58^o. Usual tilt angles associated to intra-cloud lightning leaders (attributed to TGF, at least the ones detected from space) are between ±5 and ±40 degrees with respect to the local vertical (*Lyu et al.*, 2016; *Mailyan et al.*, 2019). Figure A.4 is an illustration of qualitative arguments to justify why the TEB energy spectrum is not significantly affected by both the opening angle of the TGF and its tilt. The electrons/positrons that will be ultimately detected are only the ones that are produced between ≈ 40 and ≈ 100 km altitude (*Sarria et al.*, 2015), inside a geomagnetic field line "tube" that extends to the satellite. The energy spectrum of these electrons has no reason to change if the opening angle of the source TGF is increased or decreased. It has also no reason to change if the source TGF is slightly tilted (0^o to 5^o). If the source TGF is tilted towards the field line with larger angles, than the electron/position spectrum has no reason to change. If the beam is tilted largely away from the magnetic field "tube", then the TEB will not be detected by the satellite. For intermediate tilt angles (5^o to 40^o) we cannot provide qualitative arguments, but the effect was evaluated using simulations. We show in Figure A.5 and A.6 results of Monte-Carlo simulation assuming several opening angle values ($\sigma = 5^o, 12^o, 20^o, 30^o$) and tilt angles ($\rho = -40^o, -20^o, -10^o, -5^o, 0^o, 5^o, 10^o, 20^o, 40^o$). These simulations results confirm that the effect of varying σ_θ or ρ has indeed a very weak effect on the TEB energy spectrum.

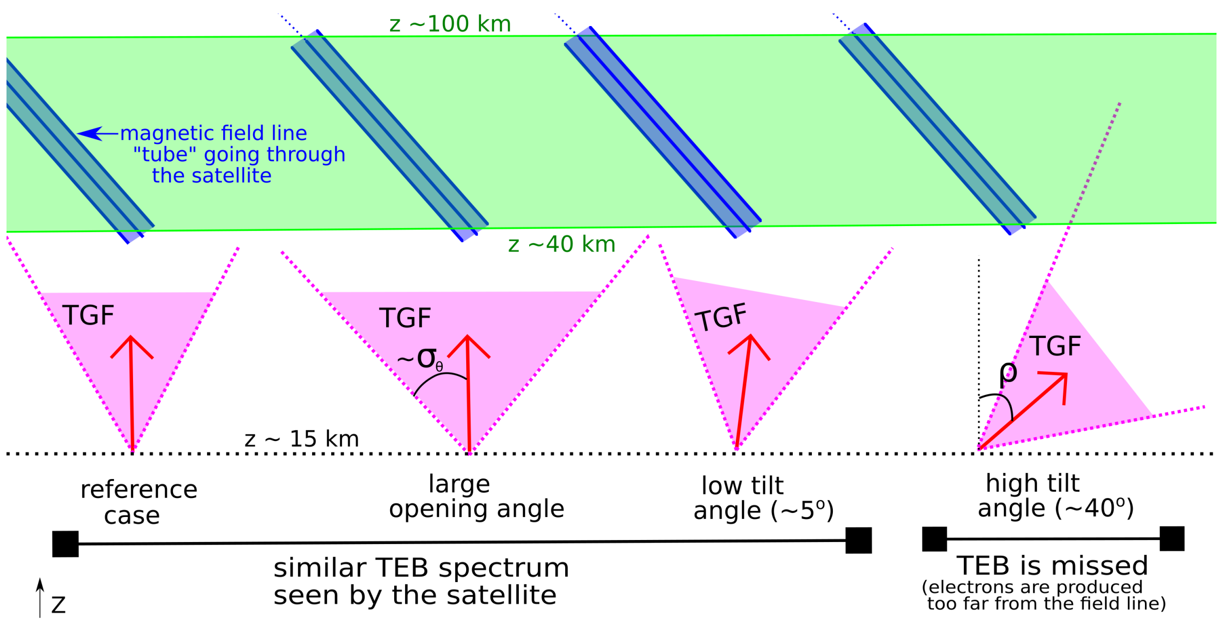

Figure A.4: Illustration of the effect of the angular distribution of the source TGF (a.k.a. beaming), i.e. when increasing the opening angle or tilting the photon beam. The source TGF is assumed to be beamed as a cone for simplicity. The electrons that are going to be eventually detected are produced between 40 and 100 km altitude along a specific geomagnetic field line tube. The energy spectrum of these electrons has no reason to change if the beaming is wider or tilted. If the tilt angle is too large, but in this case no (or very little) electrons are produced within the required area. The energy bins are chosen to contain a similar number of particles.

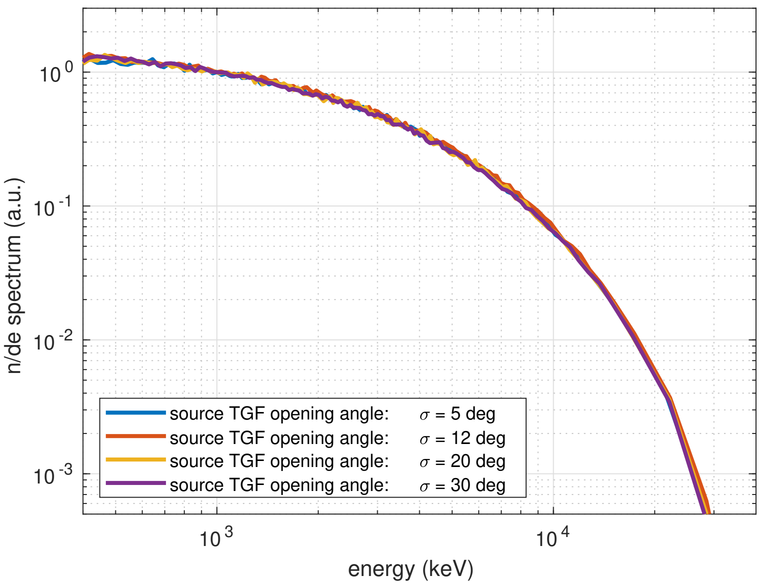

Figure A.5: Simulation results. The energy bins are chosen to contain a similar number of particles. TEB energy spectrum at satellite altitude, assuming different source TGF opening angles (σ_θ). All the tested values do not show significant difference.

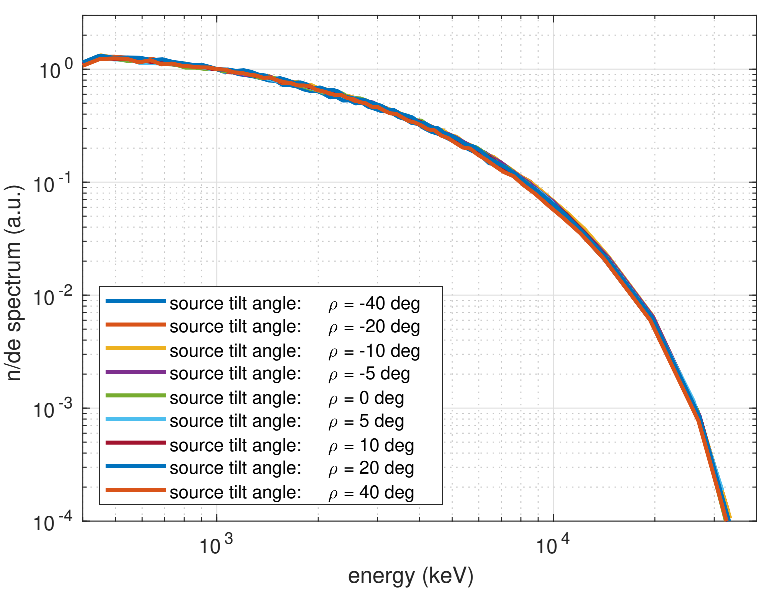

Figure A.6: Simulation results. The energy bins are chosen to contain a similar number of particles. TEB energy spectrum at satellite altitude, assuming different source TGF tilt angles (ρ) with respect to the local vertical. No significant difference is observed between the different parameters.

B Result Tables for a TGF source at 10 and 15 km altitude

In this section we present result tables of the the comparison of the tested spectral models with the measurement. In the main article, the table for a source TGF altitude of 12 km is presented, and here we present tables for a source at 10 and 15 km. We provide these tables because it is not obvious if the effect of the source TGF altitude on the TEB spectrum is weak or not, just based the TEB energy spectrum (Figure A.3). We can see that for both tables B.1 and B.2, the conclusions are the same as for the table for the 12 km case (that is Table 1 in the main article). This result confirms that the effect of the TGF source altitude is weak between 10 and 15 km and does not affect our conclusions in the main article.

Model	Effective area in cm^2		Effective area ratio	Maximum likelihood analysis result Δ_{mle}			Pearson's χ^2_r			e^+/e^- ratio
	LED	HED		LED	HED	Co.	LED	HED	Co.	
"Leader 160 MV" $\varepsilon = 4.3$ MeV $E_m = 19.2$ MeV	122.7	46.8	2.62	**0**	17.51	21.65	**0.87**	1.77	1.61	11.1%
"Leader 300 MV" $\varepsilon = 4.7$ MeV $E_m = 32$ MeV	147.5	67.6	2.18	**0**	**2.20**	6.78	**0.90**	**0.97**	**1.29**	14.6%
$\varepsilon = 6.5$ MeV $E_m = 40$ MeV	160.8	81.0	**1.98**	**0.06**	**0.18**	**2.98**	**0.90**	**0.81**	**1.26**	15.9%
$\varepsilon = 7.3$ MeV $E_m = 40$ MeV	163.5	86.0	**1.90**	**0.56**	**0**	**1.79**	**0.91**	**0.80**	**1.27**	16.9%
$\varepsilon = 8$ MeV $E_m = 40$ MeV	167.3	89.9	**1.86**	**0.17**	**0.21**	**0.99**	**0.90**	**0.81**	**1.27**	17.4%
$\varepsilon = 10$ MeV $E_m = 40$ MeV	177.7	100.3	**1.77**	**0**	**2.66**	**0**	**0.94**	**0.81**	**1.31**	19.3%
Compatibility range	n.a.		1.82±0.35	≤ 5			≤ 1.94	≤ 1.75	≤ 1.57	n.a.

Table B.1: ***For a TGF source altitude of 10 km.*** *Table summarizing the comparison of the tested spectral models with the measurement. Three main criteria are presented: the LED/HED effective area ratio, the maximum likelihood and the Pearson's χ^2_r. "Co." stands for the LED and HED combination. The compatibility range for the different criteria are also indicated. Bold values indicate compatible models for the given criterion.*

Model	Effective area in cm^2		Effective area ratio	Maximum likelihood analysis result Δ_{mle}			Pearson's χ^2_r			e^+/e^- ratio
	LED	HED		LED	HED	Co.	LED	HED	Co.	
"Leader 160 MV" $\varepsilon = 4.3\,\mathrm{MeV}$ $E_m = 19.2$ MeV	127.7	43.8	2.92	**0.06**	20.28	23.00	0.86	**1.91**	1.63	9.3%
"Leader 300 MV" $\varepsilon = 4.7\,\mathrm{MeV}$ $E_m = 32$ MeV	149.12	61.8	2.41	**0.34**	**4.33**	7.50	**0.86**	**1.00**	**1.27**	12.0%
$\varepsilon = 6.5\,\mathrm{MeV}$ $E_m = 40$ MeV	157.4	73.5	**2.14**	**0.18**	**1.29**	**3.29**	**0.88**	**0.90**	**1.26**	13.9%
$\varepsilon = 7.3\,\mathrm{MeV}$ $E_m = 40$ MeV	165.8	78.4	**2.11**	**0.37**	**0.51**	**1.97**	**0.89**	**0.83**	**1.25**	14.6%
$\varepsilon = 8\,\mathrm{MeV}$ $E_m = 40$ MeV	169.9	83.6	**2.03**	**0.05**	**0.12**	**1.09**	**0.90**	**0.84**	**1.28**	15.7%
$\varepsilon = 10\,\mathrm{MeV}$ $E_m = 40$ MeV	187.7	98.6	**1.90**	**0**	**0.50**	**0**	**0.91**	**0.81**	**1.29**	17.3%
Compatibility range	n.a.		1.82±0.35	≤ 5			≤ 1.94	≤ 1.75	≤ 1.57	n.a.

Table B.2: ***For a TGF source altitude of 15 km.*** *Table summarizing the comparison of the tested spectral models with the measurement. Three main criteria are presented: the LED/HED effective area ratio, the maximum likelihood and the Pearson's χ^2_r. "Co." stands for the LED and HED combination. The compatibility range for the different criteria are also indicated. Bold values indicate compatible models for the given criterion.*

C Spectrum comparison plot

In this section, we present the plot the spectra of the different models used to calculate the χ^2_r values in Table 1 of the main article. The source TGF is at an altitude of 12 km, has a Gaussian angular distribution with $\sigma = 20^o$ and no tilt angle (like in the main article). The showed energy binning for LED and HED is the same as the one used to calculate the χ^2_r. The results of the χ^2_r analysis are discussed in the main text.

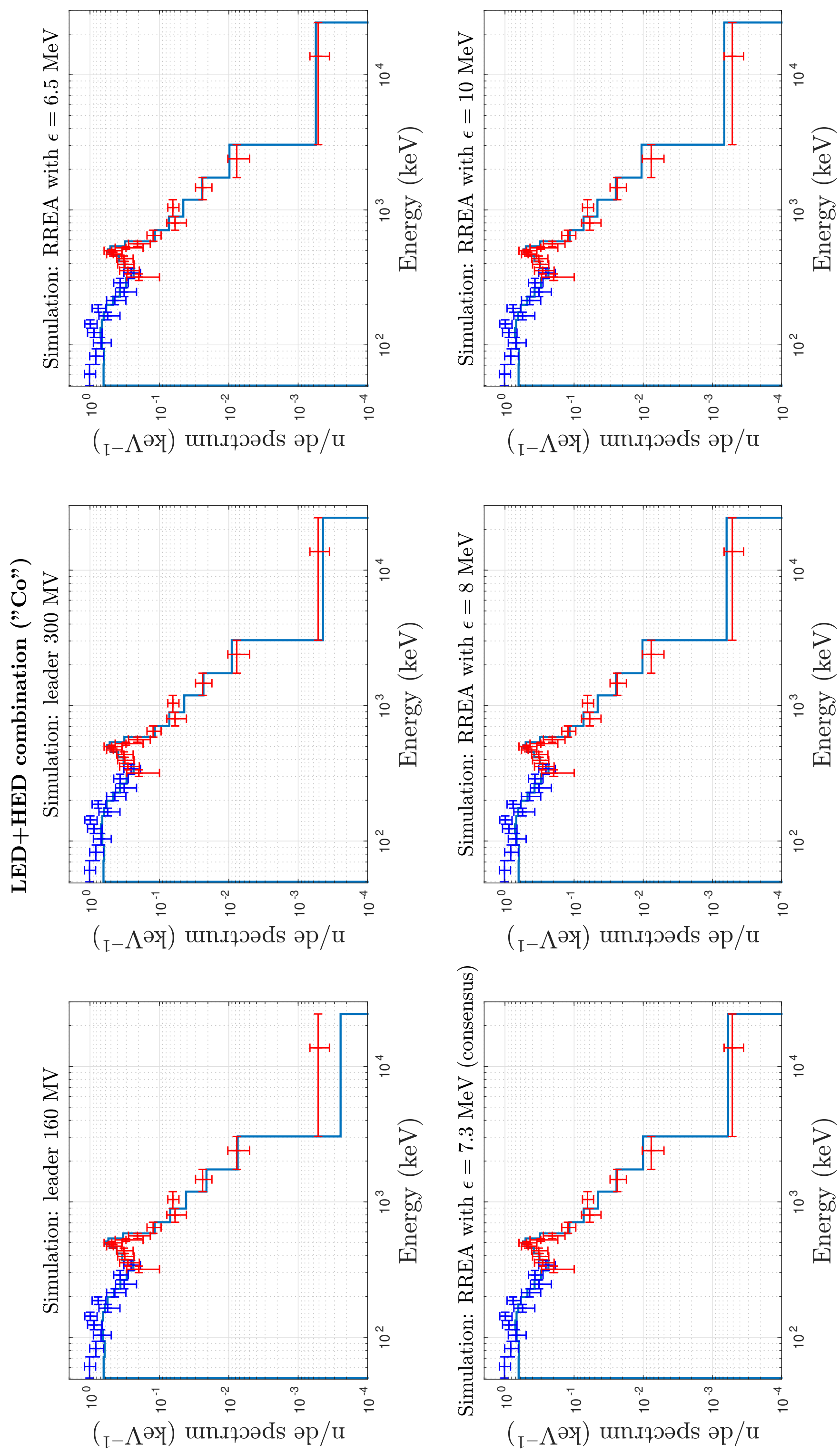

Figure C.1: Spectrum comparison between the TEB measurement, with both LED and HED, and the models described in the main article. The red and blue error bars are the measurement (identical for all subplots), and the blue histograms are the models.

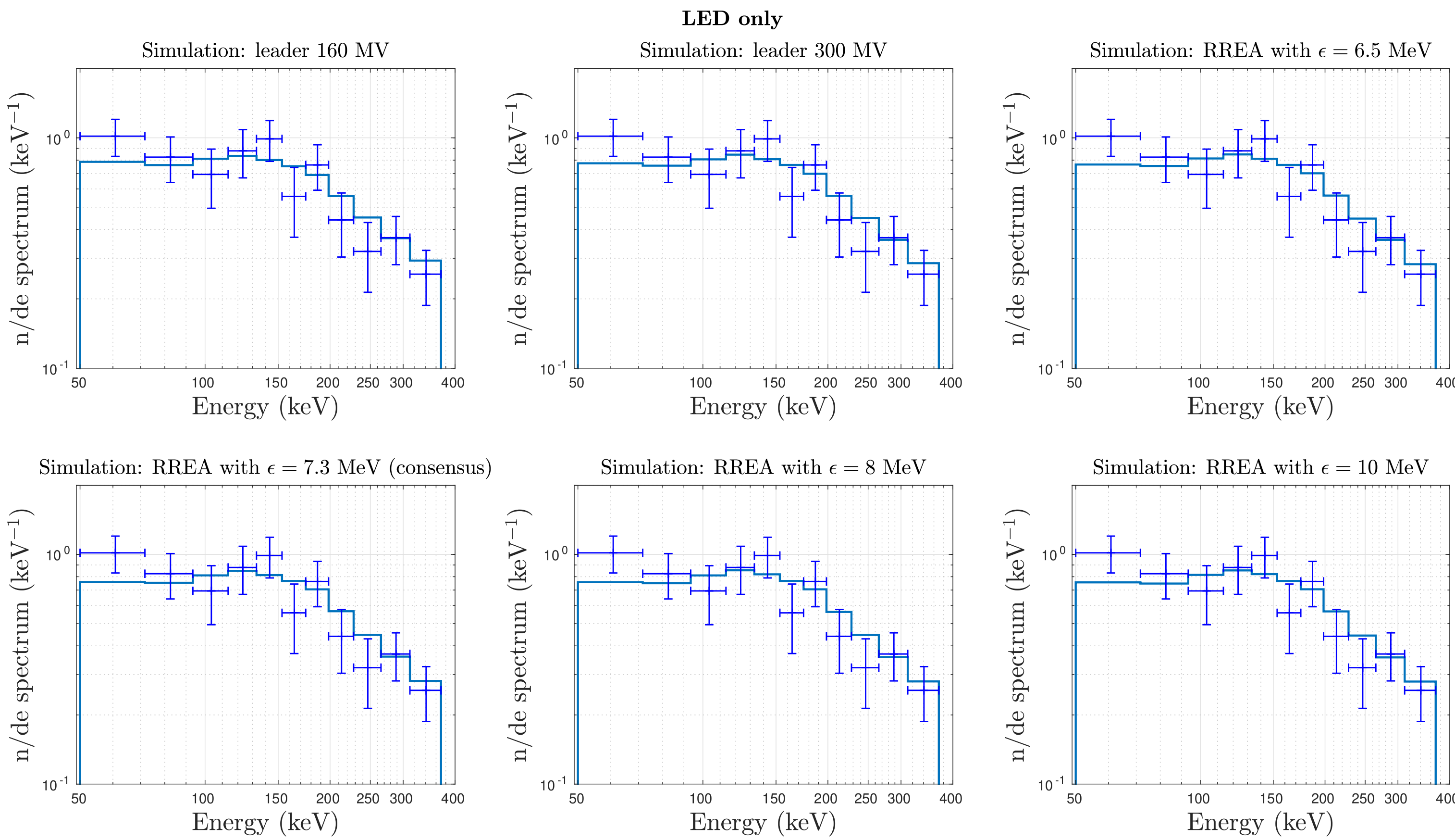

Figure C.2: Spectrum comparison between the TEB measurement, with only LED, and the models described in the main article. The blue histogram with error bars is the measurement (identical for all subplots), and the blue histograms are the models.

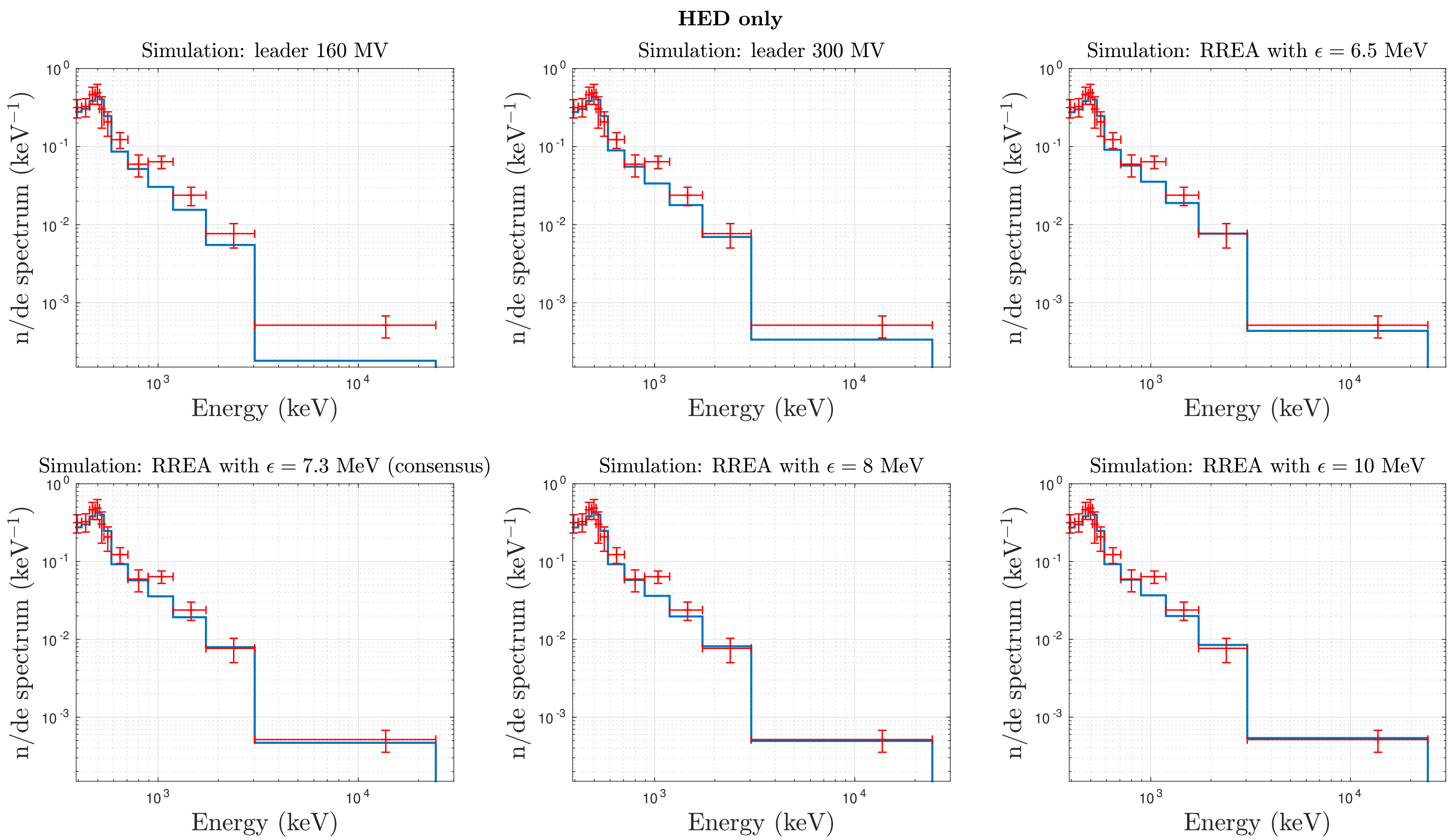

Figure C.3: Spectrum comparison between the TEB measurement, with only HED, and the models described in the main article. The red histogram with error bars is the measurement (identical for all subplots), and the blue histograms are the models.

References

Lyu, F., S. A. Cummer, G. Lu, X. Zhou, and J. Weinert, Imaging lightning intracloud initial stepped leaders by low-frequency interferometric lightning mapping array, *Geophysical Research Letters*, *43*(10), 5516–5523, doi:10.1002/2016GL069267, 2016.

Mailyan, B. G., W. Xu, S. Celestin, M. S. Briggs, J. R. Dwyer, E. S. Cramer, O. J. Roberts, and M. Stanbro, Analysis of Individual Terrestrial Gamma-Ray Flashes With Lightning Leader Models and Fermi Gamma-Ray Burst Monitor Data, *Journal of Geophysical Research (Space Physics)*, *124*(8), 7170–7183, doi:10.1029/2019JA026912, 2019.

Sarria, D., P.-L. Blelly, and F. Forme, MC-PEPTITA: A Monte Carlo model for Photon, Electron and Positron Tracking In Terrestrial Atmosphere—Application for a terrestrial gamma ray flash, *Journal of Geophysical Research (Space Physics)*, *120*(5), 3970–3986, doi:10.1002/2014JA020695, 2015.